This is the peer-reviewed, final accepted version for American Mineralogist, published by the Mineralogical Society of America.
The published version is subject to change. Cite as Authors (Year) Title. American Mineralogist, in press.
DOI: https://doi.org/10.2138/am-2022-8779. http://www.minsocam.org/

Revision 3

Don Juan Basin, Antarctica: A Chemically-Altering Environment with Martian Analog Potential

Andrew B. Foerder[1, a] Peter A. J. Englert[1, *], Janice L. Bishop[2, 3], Christian Koeberl[4], Zachary F. M. Burton[5], Shital Patel[2, 3], Everett K. Gibson[6]

[1] Hawai'i Institute of Geophysics and Planetology, University of Hawai'i at Mānoa, Honolulu, HI 96822-2336, USA

[2] SETI Institute, Mountain View, CA 94043-5139, USA

[3] NASA Ames Research Center, Moffet Field, CA 94035-1000, USA

[4] Department of Lithospheric Research, University of Vienna, Althanstrasse 14, A-1090 Vienna, Austria

[5] Department of Geological Sciences, Stanford University, Stanford, CA, 94305, USA

[6] NASA Johnson Space Center, Houston, TX 77058-3607, USA

[a] Present address: Boulder, CO

*Corresponding author: Hawai'i Institute of Geophysics and Planetology, University of Hawai'i at Mānoa, Honolulu, HI 96822-2336, USA; Email address: penglert@hawaii.edu (P.A.J. Englert)

ABSTRACT

The McMurdo Dry Valleys of Antarctica provide a testbed for alteration processes on Mars due to the cold, arid, and windy conditions. Analysis of three sediment cores collected from Don Juan Basin, Wright Valley, Antarctica, reveals that surface sediment formation is primarily dominated by physical alteration. Chemical alteration occurs sporadically in this region and is frequently indicated by the accumulation of sulfates and Cl-bearing salts. We investigated the effects of physical and chemical alteration in Don Juan Basin by considering major and trace element abundances in the sediments based on depth and location. Our results indicate inversely related chemical- and physical-alteration gradients with proximity to Don Juan Pond where the current center of the pond represents a more chemically-altering environment and the perimeter a more physically-altering one. Comparing calculated sulfate abundances for Don Juan Basin cores to rock and soil samples taken by the rover Curiosity at Gale

crater, we observed that the core from within Don Juan Pond best matches Curiosity soil sulfate abundances.

A new Chemical Index of Alteration equation that adjusts for salt dilution was also applied to the Antarctic cores and Curiosity rocks and soils. Our analysis indicates a significantly higher degree of chemical alteration than originally reported for most Antarctic and martian samples. Our investigation provides evidence for aqueous-based chemical alteration under cold, hyper-arid conditions in Don Juan Basin, Antarctica. Our work also demonstrates the analogous nature of terrestrial microenvironments to similar, local-scale sample sites on Mars, thereby supporting past or present chemical alteration on Mars.

Keywords: Mars analog; McMurdo Dry Valleys, Antarctica; chemical alteration; geochemistry; spectroscopy; mineralogy

INTRODUCTION

This study aims to investigate the type and degree of alteration for samples collected at multiple depths in soil pits in and around Don Juan Pond (DJP) of the McMurdo Dry Valleys (MDV) region to better understand the processes operating in the basin. Alteration signatures are determined through elemental and mineralogical analysis and are organized into two general modes: physical and chemical. Based on the frigid temperatures, high winds, and the extremely dry nature of the MDV, physical alteration is assumed to dominate and likely manifests primarily as sediment-mixing, freeze-thaw cycling, and aeolian abrasion (e.g., Nichols, 2009). Chemical alteration is suggested to be operating on a secondary scale and is primarily observed as an effect of standing water and salt accumulations (e.g., Nichols, 2009). Sediment provenance, surface, and subsurface processes are considered together with chemical and mineralogical data to provide information on alteration processes.

Due to their similar environmental conditions, the characterization of analog sites in the MDV can provide insights to constrain the geochemical and geomorphological history of Mars. In this study, we investigate relationships among soil pit samples from three sites in Wright Valley in or near DJP to determine variations due to distance from the center of the pond and depth below the surface. We use this data to assess the relative importance of chemical and physical alteration in Wright Valley and also

to provide geochemical and mineralogical results for comparison with data collected at Mars. Major element abundances have been measured at several sites on the surface of Mars (e.g., Clark, 1993; McSween, 2002; Velbel, 2012; McLennan et al., 2014; Vaniman et al., 2014; Gellert and Yen, 2019), documenting a basaltic planet with high salt contents and aqueous alteration at some locations. Elemental analyses and X-Ray Diffraction (XRD) at Gale crater indicate the presence of abundant, varying species of Ca-sulfates (e.g., McLennan et al., 2013; Nahcon et al., 2014; Vaniman et al., 2018; Tu et al., 2021), similar to the MDV. Additional evidence for past aqueous activity on Mars is available through mineralogy determined from orbital reflectance spectroscopy (e.g., Murchie et al., 2019). Thus, one objective of analyzing the elemental, chemical, and mineralogical data of Antarctic sediments at variable depths and distances from an evaporite pond is to improve the understanding of spatial evaporative and subterraneous aqueous processes on Mars.

CLIMATE AND GEOLOGY OF THE MCMURDO DRY VALLEYS

The continent of Antarctica (Figure 1a) is a remote, desolate, and inhospitable landscape with an area of about 14.2 million km^2 that is largely covered by ice. Regions free of ice and snow make up less than 710,000 km^2 or 5 % of the area of the continent, with the ice-free "dry" valleys making up only 4,800 km^2 or 0.03 % (Harris, 1981). The location of McMurdo Station, a United States Antarctic research center on the southern tip of Ross Island, has allowed for past and present studies of the MDV (Figure 1b). Regional geology of the MDV consists largely of a basement granitoid complex (Gunn and Warren 1962; Grindley and Warren, 1964; Peterson and Marsh, 2008), a sandstone part of the Beacon Supergroup (Ferrar, 1907; Peterson and Marsh, 2008), and sequences of quarts diabase sills and dikes known as Ferrar Dolerite (Harrington, 1958; Gunn and Warren, 1962; Morrison 1989; Peterson and Marsh, 2008).

Climate plays a critical role in maintaining the Valley's lack of ice. Mean annual precipitation, entirely as snow, ranges from 5 to 10 cm in valley bottoms (Thompson, 1971), while annual sublimation is at least 50 cm (Ragotzkie, 1964; Yusa, 1972; Anderton, 1976; Chinn, 1976). Annual temperatures in central Wright Valley (Figure 2a) are between -17 and -22 °C, with lows reaching -55 °C during winter, and highs reaching 10 °C for short periods in the late summer. Higher elevations, comparatively, are

much colder, with temperatures rarely exceeding 0 °C above 1000 m (Bull, 1966; Doran et al., 2002). Mean soil temperatures, the closest measured near the Lake Vanda station, roughly 8 km to the northeast, are approximately -20 °C at a depth of 46 cm (Thompson et al., 1971b; McLeod et al., 2009; Obryk et al., 2020).

As a result of the hyper-arid and frigid environment, the prevalence/presence of liquid surface water is limited. Under the appropriate thermal and chemical conditions, liquid water does occur seasonally at a local level (Harris, 1980; Harris and Cartwright, 1981; Chinn 1993; Doran et al., 1994). Hypersaline, ice-covered lakes, such as Lake Vanda, are major features of the MDV. However, DJP (Figure 2b) of Upper Wright Valley, the focus of this study, is unique as a hypersaline, perennially liquid water pond.

DON JUAN POND

DJP (Figure 2b), found in Don Juan Basin, has likely been ice-free for as much as 2 million years (Calkin et al., 1970), suggesting that standing water and associated aqueous processes may have been active for a similar amount of time. The glacial history of the region supports this timeline, as the East Antarctic outlet glacier has not expanded through Wright Valley, and hence could not have occupied the Dry Valleys sector of the Transantarctic Mountains any time in the past 3.8 million years (Hall et al., 1997). Rather, there has been a moderate Pliocene expansion of local cold-based alpine glaciers paired with continuous cold-desert conditions in Wright Valley (Calkin et al., 1970; Hall et al., 1997).

DJP is the second most saline body of water known on Earth at 24-40 % $CaCl_2$ (Torii and Osaka, 1965; Torii et al.,1980; Pérez and Chebude, 2017) and was discovered in 1961 (Meyer et al., 1962). The pond and basin contain significantly elevated levels of calcium salts in the form of antarctictite ($CaCl_2 \cdot 6H_2O$) (Torii et al., 1977) and gypsum ($CaSO_4 \cdot 2H_2O$), as well as elevated halite (NaCl) that leave a “bathtub ring” of salt encrustation around the perimeter (Oberts, 1973). Aqueous processes and the brine chemistry depend on the regional water system and several schools of thought describe potential sources of water for the formation of DJP: 1) stream input from the western lobe of a rock glacier; 2) stream input from melted, frozen ground; 3) upwelling of a deep groundwater dolerite aquifer; and 4) active

124 layer transport atop the permafrost table within the colluvium end of the pond (Harris, 1981; Harris and
125 Cartwright, 1981; Dickson et al., 2013).
126
127 The first model—stream input from the western lobe of a rock glacier during the summer (Harris and
128 Cartwright, 1981; Hassinger et al., 1983; Morgan et al., 2008, Toner et al., 2022)—could contribute both
129 an aqueous and ionic input (Harris and Cartwright, 1981). Winsor et al., 2020, conducted ionic analyses
130 on soil leachate of samples from the lower rock glacier (western lobe) and reported high levels of Ca^{2+},
131 Cl^-, F^-, K^+, SO_4^{2-}, and Na^+ ions that trend towards the higher levels measured at DJP, consistent with
132 stream input from the western lobe that then experiences evaporative concentration closer to the pond.
133
134 The second model includes occasional freshwater stream inputs that could provide significant volumes
135 of water, interpreted as the product of melting frozen ground (Harris and Cartwright, 1981). Other
136 processes include landslides, debris flows, and/or surface streaks that may be related to the Recurring
137 Slope Lineae (RSL) on Mars (Harris and Cartwright, 1981; Dickson et al., 2013; Toner et al., 2022).
138
139 The third model—the upwelling of a deep groundwater aquifer—is still debated. It can provide both a
140 source of water that maintains the pond and a source of calcium that originates from aqueous interaction
141 with an underlying dolerite deposit (Harris, 1981). The calcium would then be able to combine with
142 chlorides that are introduced through marine aerosols, and subsequent precipitation and/or stream input
143 to form calcium chloride ($CaCl_2$). Electrical depth soundings (McGinnis et al., 1971; McGinnis, 1973)
144 and seismic profiles (McGinnis, 1973) have shown that the terrain beneath the pond is unfrozen to a
145 depth of 30 m, sloping westward to 60 m. The geologic sequence was interpreted to be unfrozen
146 granodiorite basement rock superposed by a dolerite deposit, and then a wet, sandy, lacustrine deposit
147 directly beneath the pond (McGinnis, 1973; Harris, 1981). From the Dry Valley Drilling Project
148 (DVDP), samples of water showed that subsurface water beneath the pond was enriched with $CaCl_2$ in
149 contrast to surface concentrations that can be explained by the evaporative concentration of the salts.
150 This hypothesis is favored by Cartwright and Harris (1981). Additionally, Toner (2012) reports that the
151 amount of $CaCl_2$ that can be produced by exchange reactions is consistent with estimated amounts of
152 $CaCl_2$ in groundwaters beneath DJP. This suggests that cation exchange reactions can explain the Ca and
153 Cl-enriched composition of DJP and other brines in the Dry Valleys. Harris (1981) finds that the

discharge of saline groundwater from a subterraneous dolerite aquifer to the surface is likely the primary source of the annual water supply to the pond.

Finally, it has been speculated that active layer transport occurs atop the permafrost table within the colluvium end of the pond. This is seen as water tracks/wet streaks at the surface (Cartwright and Harris, 1981; Hastings et al., 1989; McNamara et al., 1999; Head et al., 2007; Levy et al., 2011, Toner et al., 2022). These are areas of high soil moisture that act as downslope paths for saline liquids on top of the permafrost table. Such liquids are enriched in Ca^{2+} (Winsor et al., 2020), which further bolsters this hypothesis.

Many of the sediments across the MDV are classified as Typic Anhyorthels (McLeod et al., 2009). According to the USDA Soil Taxonomy, these are soils that have accumulations of salts, including gypsum and calcium carbonate, but insufficient quantities to meet the criteria for a calcic, gypsic, petrogypsic, or salic horizon within the upper 100 cm. In addition, they do not have a lithic contact within 50 cm of the mineral sediment surface, an organic surface layer that thins and thickens in relationship to microrelief, nor do they have andic properties (McLeod et al., 2009). The sediments marginal to DJP contain sufficient salt to satisfy the requirements for a salic horizon and are continuously kept under reducing conditions, therefore they are classified as “Salic Aquorthels” (McLeod et al., 2009). The sediments found in low areas of the North and South Forks of Wright Valley and on the outer extent of DJP are predominantly classified as “Salic Haplorthels”. These sediments are chemically similar to Salic Aquorthels but do not possess aquic conditions within 50 cm of the sediment surface (McLeod et al., 2009).

METHODS

Sample Collection and Preparation

Samples were collected from three locations in Don Juan Basin (Figure 2b) during the 1979-80 field season using drive tubes similar to those used by the Apollo missions (Gibson et al., 1983). Larger quantities of materials were obtained from trenches excavated directly adjacent to the respective drive tube core locations for extended analysis. Our study focused primarily on these scooped soil pit samples.

For simplicity and to help manage sample locations, we refer to these soil pit samples in relation to the drive tube core number where they were collected: JB1124-26 (Core 2074), JB1129-33 (Core 33), and JB1134-38 (Core 39). Core 2074 is situated in the center of DJP, while Core 33 is located about 150 m to the southwest and Core 39 is located about 300 m to the southwest, providing information radially outward from DJP (Figure 2b). Based on data from Harris and Cartwright (1981) the center of DJP, where core 2074 is located, is approximately 116 m above sea level, while the locations of cores 33 and 39 are at elevations of approximately 116.4 m and 117 m, respectively. These three sample sites provide data on extremely local environments or "microenvironments" within the Don Juan Basin.

Table 1 provides locations of the sample collection sites relative to DJP, field notes about the samples, sampling depths, and sample IDs. The drive tube core at sample site 2074 did not reach the permafrost layer although it was taken to a depth of 31 cm. The drive tube cores at sample sites 33 and 39 did penetrate the permafrost layers, which were found at depths of 27 and 25 cm, respectively. For the soil pit samples collected adjacent to the cores 2074, 33, and 39, the approximate depths from the surface were estimated in the field, often at intervals of a few centimeters. The samples from the core 2074 sample site include surface material with white encrustations attributed to evaporites (JB1126), near-surface material without these white crusts (JB1124), and scooped material down to a depth of ~10 cm (JB1125). The samples from the core 33 sample site include material scooped from the surface (JB1129) scooped material and several depths down to about 16-20 cm (JB1133). Similarly, the samples from the core 39 sample site include material scooped from the surface (JB1134) and material scooped at several intervals down ~15-16 cm (JB1138). Aliquots of each sample were gently crushed using a mortar and pestle until all the ground material passed through a 125 μm sieve. This ensured that all minerals were included in the <125 μm size fraction and not just the softer minerals.

Elemental Analyses

Major, minor, and trace element abundances of the <125 μm sediment size fraction were measured by ACME Analytical Laboratories (now Bureau Veritas) in Vancouver, B.C., Canada, using X-ray fluorescence (XRF). Sulfur measurements and Loss on Ignition (LOI) at 1000 °C were also conducted at ACME Labs using LECO combustion. These data are reported in Table 2. SO_3 concentrations were calculated from the measured sulfur (S) data. Specific sulfate and chloride abundances for $CaSO_4$,

Na_2SO_4, K_2SO_4, $MgSO_4$, NaCl, and $CaCl_2$ were calculated by converting CaO, K_2O, Na_2O, MgO wt. % to mole fraction and multiplying oxide moles by the molecular weight of each in its sulfate form to attain wt. % sulfate and chloride. Additional minor and trace element abundances, including those of the rare earth elements, were measured by instrumental neutron activation analysis (INAA) at the Department of Lithospheric Research, University of Vienna, Austria, and are reported in Table 3. INAA is a technique used to determine the concentrations of trace and major elements with high neutron capture cross sections in a variety of matrices. The sample is exposed to a neutron flux that produces radioactive nuclides that emit gamma rays characteristic of each element. The intensity of these gamma rays is then compared with those emitted by a standard to allow for quantitative analysis. Additional details of this method, including elemental precision and accuracy, are described by Koeberl and co-workers (Koeberl, 1993; Mader and Koeberl, 2009).

Reflectance Spectroscopy

Visible near-infrared (VNIR) spectra were measured from 0.35-2.5 μm for the coarse (<125 μm) size fractions of undried grains at the SETI Institute with an ASD FieldSpecPro reflectance spectrometer under ambient conditions relative to Spectralon. This was conducted to ensure consistency for the bulk and fine-grained samples. Reflectance spectra were also measured at the Reflectance Experiment Laboratory (RELAB) at Brown University of the <125 μm size fraction under controlled dry conditions. The RELAB spectra are composites prepared from bidirectional VNIR and Fourier Transform Infrared (FTIR) data. The VNIR spectra were measured from 0.3-2.5 μm under ambient conditions relative to halon. The FTIR spectra were collected from 1-25 (or 50) μm or 10,000 to 400 (or 200) cm^{-1} using a Nicolet spectrometer in an off-axis biconical configuration under an H_2O- and CO_2-purged environment relative to a rough gold standard as in previous studies (e.g., Bishop et al., 2014a). The spectra were connected near 1.2 μm to produce reflectance spectra of the samples in a dry environment without adsorbed water.

X-ray Diffraction

Mineralogical analysis was conducted on the <125 μm size fraction of the samples using an Olympus Terra-166 XRD instrument, which was designed as a field XRD unit (e.g., Sarrazin et al., 2005) and

247 performs similarly to the CheMin instrument on Mars (e.g., Blake et al., 2013). XRD analysis of most
248 samples in this study was conducted on freshly ground samples that were preserved in sealed containers
249 and not dried prior to the analyses. Some sample aliquots containing hygroscopic samples were partly
250 dried at <100 ºC for separate XRD analysis due to the sticky nature of the original grains. Within the
251 limits of uncertainty, there was no permanent change of composition recorded, and samples regained
252 moisture to their original level. XRD peaks were matched with mineral standard databases using
253 Olympus proprietary software which allowed for further qualitative and quantitative analysis. Results
254 are used as a qualitative indicator of minerals present in this study.
255
256 **Water-soluble Ions**
257
258 Water-soluble anions and cations were measured on samples from the drive tube cores soon after the
259 samples were collected (Gibson et al., 1983) and are provided in Table 4. This is different from the other
260 analyses; however, the chemistry is assumed to be similar in the drive tube core and the scooped
261 samples at the depths investigated. Water-soluble anions were measured by ion-selective electrode
262 chromatography techniques using a 1:5 soil-water extraction and water-soluble cations were measured
263 by atomic absorption spectrophotometry and emission flame photometry following procedures by Small
264 et al. (1975). However, this may underestimate the amount of some ions (Bao et al., 2000). The original
265 data tables from these measurements were available for core 39, but not for core 33 or core 2074. This
266 required careful derivation of values for the core 33 and core 2074 samples from an original graph of
267 these data. Although the water-soluble anion and cation data represent approximate values, they provide
268 information on general trends in the compositions of these samples with depth.
269
270 **Characterizing Sediment Alteration**
271
272 Our principal approach to characterizing sediment alteration is through the analysis of major, minor, and
273 trace element abundances, including rare earth elements, and the mineralogical composition of samples
274 from microenvironments. A specific, quantitative method to evaluate degree of chemical alteration that
275 uses major element abundances is the Chemical Index of Alteration (CIA). The CIA is used to assess the
276 effects of physical versus chemical alteration in pedogenesis. It reflects the proportions of primary and
277 secondary minerals in bulk samples, providing a means to order samples (Nesbitt and Young, 1982;

This is the peer-reviewed, final accepted version for American Mineralogist, published by the Mineralogical Society of America.
The published version is subject to change. Cite as Authors (Year) Title. American Mineralogist, in press.
DOI: https://doi.org/10.2138/am-2022-8779. http://www.minsocam.org/

Krissek and Kyle, 2000; Sheldon and Tabor, 2009; Li and Yang, 2010). Additionally, the CIA can be used to assess the degree and process of alteration (Nesbitt and Young, 1982; Fedo et al., 1995) by comparing samples to source rock. The CIA is based on the mobility of major elements Al, Ca, Na, and K. Fresh basalts have a CIA range of 30-45; fresh granites and granodiorites have a CIA range of 45-55; feldspars, 50; illite, 75-90; and kaolinite, 100 (Nesbitt and Young, 1982; Fedo at al., 1995). The following equation defines the CIA (Nesbitt and Young, 1982):

$$\mathrm{CIA} = 100 \cdot \frac{\mathrm{Al_2O_3}}{\mathrm{Al_2O_3} + \mathrm{CaO^*} + \mathrm{Na_2O} + \mathrm{K_2O}} \ (molar)$$

where the sample abundance of each oxide is divided by the molecular weight of each oxide. CaO* is the amount of CaO in the silicate fraction of the samples. The Nesbitt and Young (1982) definition of the CIA assumes that in regular, non-arid environments, salts do not accumulate and chemically-altered ions will be transported out of the sample. CIA values calculated for samples with secondary minerals—such as sulfates or chlorides—are likely reduced, making the sample appear less weathered than it is. Though methods have been developed to evaluate and account for the effect of sediment salinization on the degree of chemical alteration (e.g. Parker, 1970; Fedo et al., 1995; Sheldon and Tabor, 2009; Liu et al., 2021), they prove restrictive to our cause. It would be useful to quantify chemical alteration in the hyperarid MDV if the effect of accumulated non-mobilized salts can be accounted for. Therefore, we propose a process by which to correct the CIA equation in a first-order approximation that assumes all SO_3 and Cl^- is present as $CaSO_4$, K_2SO_4, $MgSO_4$, Na_2SO_4, NaCl, or $CaCl_2$. We acknowledge that this assumption is an oversimplification as there is a possibility that some of the salts are exogenic and not derived from the local parent material. XRD analyses reveal the presence of a small fraction of unaltered parent materials, however, the salt correction is only intended to provide a means by which to better understand the general degree of chemical alteration taking place at the sample sites. The order of the sulfate and chloride species follows the respective K_{sp} (solubility constant product) for each compound. In other words, the order reflects the preference of precipitation. To correct the CIA, the following steps are taken: 1) Convert CaO, K_2O, Na_2O, and MgO wt % to mole fraction. MgO is included due to its relevance on Mars (kieserite) 2) Multiply oxide moles by the molecular weight of each in its sulfate form to attain wt % sulfate and chloride: $CaSO_4$, K_2SO_4, $MgSO_4$, Na_2SO_4, NaCl, $CaCl_2$ 3) Subtract $CaSO_4$, K_2SO_4, $MgSO_4$, Na_2SO_4, NaCl, and $CaCl_2$ wt % from each oxide's original % abundance, 4)

This is the peer-reviewed, final accepted version for American Mineralogist, published by the Mineralogical Society of America.
The published version is subject to change. Cite as Authors (Year) Title. American Mineralogist, in press.
DOI: https://doi.org/10.2138/am-2022-8779. http://www.minsocam.org/

Insert the new value of oxide wt % into CIA equation to determine the undiluted CIA value. A proposed corrected CIA equation is shown below

$$\mathrm{CIA}_{Salt} = 100 \cdot \frac{\mathrm{Al_2O_3}}{\mathrm{Al_2O_3} + [\mathrm{CaO^*}]_{SC} + [\mathrm{Na_2O}]_{SC} + [\mathrm{K_2O}]_S + [\mathrm{MgO}]_S} \ (molar)$$

where subscripts *S* and *C* are the oxide abundances after subtracting respective sulfate and chloride abundances. If after subtracting $CaSO_4$, K_2SO_4, Na_2SO_4, $MgSO_4$, and $CaCl_2$ wt % from each oxide's original wt % abundance, the value returned is negative, the oxide is assumed to be completely consumed by SO_3 or Cl^- to form the oxide's sulfate or chloride form. In this instance, CaO, K_2O, Na_2O, and MgO are inserted into the CIA equation as "0". This salt-corrected CIA equation should provide a qualitative (and quantitative) means to establish the degree of chemical alteration in the soils analyzed. The degree and process of alteration are also assessed through the analysis and comparison of select elements and elemental ratios that are diagnostic of particular source rocks. Due to their high field strengths, Ti, Zr, and rare earth elements (REE) are less mobile than elements such as K and Ca. REE patterns have also been used to determine sediment provenance because basic rocks contain low Light REE/Heavy REE (LREE/HREE) ratios and no Eu anomalies, whereas more silicic rocks usually contain higher LREE/HREE ratios and negative Eu anomalies (Cullers and Graf, 1984). Based on this, certain REE patterns and abundances can be used to infer the degree/type of alteration (Nesbitt and Markovics, 1997).

RESULTS

In the MDV, physical alteration is likely expressed primarily as sediment mixing, believed to be a result of aeolian transport and mass wasting. Freeze-thaw processes are also believed to contribute to physical alteration across the region. Chemical alteration is primarily expressed as salt precipitates because of evaporation from the limited moisture in the region. Here we focus on the influence of hypersalinity that permits water to remain stable and promotes chemical alteration at the surface and near-surface.

Elemental, Soluble, and Mineral Abundances

Analytical results obtained for Don Juan Basin core samples are provided in Tables 2 through 5. Results are presented and discussed comprehensively for each of the Don Juan Basin cores as well as cumulatively at the end of the section. Table 2 provides major and minor element oxide abundances predominantly measured by XRF. Table 3 provides major, minor, and trace elements determined by INAA. Table 4 provides soluble anion abundances determined by ion-selective electrode analysis techniques, and Table 5 provides qualitative mineralogy results determined by XRD and reflectance spectroscopy.

Table S1, found in Supplementary Materials, displays the correlation between two methods, INAA and XRF, for measuring elemental abundances of Na, K, and Fe oxides. INAA oxide abundances were calculated from elemental abundances. Evaluation of the two methods exhibits good agreement with <20 % difference in oxide abundance across nearly all cores. For consistency, we have chosen to use INAA-derived abundances for Na, K, and Fe, as that method relies on minimal processing, and, in the case of K, on counting ^{40}K decay gamma rays.

DISCUSSION

Soil Pit Samples Near Core 2074

Only the core 2074 soil pit samples at depths of 1-2 and 8-10 cm (JB1124 and JB1125), respectively, are discussed in detail because sample JB1126 (0-1 cm) was a smaller volume and is primarily salt. Due to the limited amount of material available for this sample, fewer analyses were possible. For both JB1124 and JB1125, the depletion in what are generally considered immobile elements (e.g., Cu, Ti, Zn, Zr) suggests that sediments from the core 2074 sample site have experienced chemical alteration. Depletion of the most soluble and more mobile ions, such as Na, Ca, and K, is expected as there is little source rock remaining in which the most soluble ions would have high abundances. Th, Ba, and Sr abundances for the core 2074 soil pit samples are generally lower compared to soil pit samples collected near cores 33 and 39 (see Table 3), as are their normalized ratios K/Th (0.61-0.67) and oxide ratios Al_2O_3/TiO_2 (19.1-22.3). U abundance, however, is on average highest at the core 2074 sample site and tapers off

with distance from the pond. The JB1126 uranium (U) abundance (1.61 ppm) compares well with those of surface samples at the core 33 (1.45 ppm) and core 39 (1.14 ppm) sample sites. Interestingly, there is U enhancement in the top 2 cm (3.03 ppm) which is approximately twice the abundance of samples at the soil pits at cores 33 (1.45 ppm) and 39 (1.14 ppm) at similar depths (Table 3). The samples at the core 2074 sample site provide an excellent example of lower-than-expected element abundance, likely due to a strong dilution effect from salts. Higher average U abundance in at the core 2074 sample site could be a result of stream input from the western lobe of a rock glacier.

Rare Earth Element abundances (REE) are normalized to C1-chondrite averages per Taylor and McLennan (1985). Light Rare Earth Element abundances at the core 2074 soil pit sample site have lower concentrations but show a similar trend compared to the core 33 and 39 sample sites (see Figure 3). The three core 2074 soil pit samples exhibit a negative Eu anomaly, which is typically attributed to CaO and Na_2O depletion, which, in turn, could be due to plagioclase weathering (Nyakairu and Koeberl, 2001). All samples have lower-than-expected Tb abundances. Under special circumstances, Tb can exist as a 4+ ion, similar in radius to the 4+ ions of Zr, Hf, U, and Th; this may influence the Tb abundances. REE abundances also provide diagnostic information for the degree of chemical alteration (as in Taylor and McLennan, 1985) because of their relative immobility and insolubility. The downward trend in REE abundances (including major and trace elements) from samples located at the core 2074 sample site to those at the core 39 sample site strongly suggests active chemical alteration at the center of DJP (see Figure 3).

Nearly all depth profiles and surface samples of Don Juan Basin exhibit sulfates, including thenardite, anhydrite, and gypsum (see Table 5). Gypsum and anhydrite are the dominant sulfates, which is expected, based on the solubility products of (Ca, K_2, Mg, Na_2) · SO_4^{2-}. Mineralogical analysis of samples from the core 2074 sample site shows gypsum and abundant anhydrite in the broad absorption band at about 4.7 μm for both JB1124 (1-2 cm) and JB1125 (8-10 cm) (Figure 5a) compared with spectra of Ca sulfate minerals (Bishop et al., 2014b). Figure 5b confirms the presence of gypsum at about 1700 cm^{-1} and anhydrite at about 1200, 1450, and 1600 cm^{-1}. Table 5 summarizes minerals in Don Juan Basin core samples that have been identified by spectral reflectance and XRD measurements and also shows the possible presence of quartz and hydrated ferric oxide in samples JB1124 and JB1125.

The presence of evaporites suggests the existence, past or present, of an aqueous solution, which suggests chemical alteration.

The soluble ion distribution (Table 4 and Figure 4a) throughout Core 2074 shows relatively constant abundances of Na^+, Ca^{2+}, and Cl^- with depth, except for a significant drop in Na^+ from the surface sample to 0.5 cm depth. Na^+ abundances are low compared to Ca^{2+} and Cl^-, so it is unlikely that NaCl is a major component in Core 2074, although its presence was reported (Harris, 1982).

Soil Pit Samples Near Core 33

The soil pit samples collected near core 33 show little variation in major element abundance throughout the depth profile. However, these samples are enriched with Na and K compared to samples at the core 2074 sample site, suggesting the presence of unaltered source rock. Th and Ba abundances are elevated in these samples compared to those at the core 2074 sample site, which supports this hypothesis and strongly suggests that chemical alteration occurs to a lesser degree here than at the core 2074 sample site. The highest abundances of major elements and oxides are seen between 4-10 cm in depth. Normalized K/Th values (Figure 9) range from 0.56 (JB1133, 16-20 cm) to 0.86 (JB1132, 12-14 cm). JB1133 and JB1130 (0.67, 3-4 cm) are within the range of normalized K/Th values (0.61-0.67) in Core 2074. This could imply enhanced alteration at these depths in Core 33.

XRD analysis of the core 33 soil pit samples (Table 5) identifies quartz and albite in all but the 3-10 cm depth range. This range notably exhibits the most salt in JB1130 (3-4 cm) and JB1131 (8-10 cm), as also observed by Gibson et al. (1983) on Prospect Mesa sample sites (Central Wright Valley). JB1130 contains halite, thenardite, and anhydrite, corroborating some of the lowest reported abundances of albite and quartz. JB1131 also contains thenardite and anhydrite, but no halite. Low albite and quartz abundances in JB1130 and JB1131 are accompanied by higher abundances of orthoclase. The relatively low abundances of quartz and albite could be due to the presence of salts contributing to a dilution effect, changing the ratios of the bulk sample. However, relative REE enrichment in JB1131, as compared to the samples from the core 2074 sample site, could suggest more active alteration (Figure 3).

Reflectance spectra of the soil pit samples at the core 33 sample site (Figure 6 and Table 5) were compared with laboratory spectra of minerals (e.g., Bishop, 2019; Lane and Bishop, 2019) expected in the MDV based on previous studies (e.g. Bishop et al., 2014a). These spectra show a strong band near 2.9-3.0 μm due to bound water, Si-O stretching vibrations near 1090 and 1215 cm^{-1} (~ 8.3 and 9.2 μm), as well as overtones and combinations near 4-5 μm, suggestive of quartz. A broad Fe band near 1 μm is due to pyroxene, and bands near 1.2 and 2 μm are attributed to bassanite ($CaSO_4 \cdot 1/2H_2O$). A strong band at 4.68 μm for sample JB1132 (8-10 cm depth) indicates the presence of anhydrite (Bishop et al., 2014b). Additional weak bands near 2.35 and 2.45 μm are due to OH bands in mica (e.g., biotite) or actinolites (e.g., tremolite) that are likely part of the primary material, as discussed in Bishop et al. (2013) for other MDV sediments. Minor amounts of poorly crystalline ferric oxide-bearing components (e.g., ferrihydrite) are also present in the upper layers, which might account for deeper water bands and shifts in the ~ 1 μm band towards lower wavelengths.

The soluble ion distribution in Core 33 (Table 4 and Figure 4b) resembles that of Core 2074, exhibiting little difference in Ca^{2+} and Cl^- abundance, and comparatively low Na^+ abundance. Again, NaCl is unlikely a major component of Core 33, but is still reported. Cl^- abundances at Core 33 are approximately half of those from Core 2074, with the upper 2-3 cm exhibiting a Cl^- depletion.

REE analysis of the soil pit samples near core 33 (Figure 3) shows a pattern similar to that of other sites, but with higher abundances than the samples near core 2074 and overlapping/lower abundances when compared to samples at the core 39 sample site. A negative Eu anomaly is exhibited in all samples except for JB1132 (12-14 cm). There is a comparatively high abundance of Tm in JB1133 (16-20 cm). CaO and Na_2O depletion attributed to plagioclase weathering could be the reason for the observed negative Eu anomaly (Nyakairu and Koeberl, 2001). REE abundance is highest between 3-4 and 8-10 cm and follows the trend observed for the major elements. Based on the abundance of major and trace (REE included) elements, physical alteration is favored throughout the soil pit with chemical alteration occurring at a depth of 4-10 cm.

458 **Soil Pit Samples Near Core 39**

459

460 The core 39 soil pit samples show relative enrichment in major ions such as Na and K compared to the
461 samples at the core 2074 sample site (Table 3), suggesting more source rock in the sediments and less
462 alteration. There is little variation in oxide abundance throughout the soil profile (Table 2). Anomalous
463 cases are seen in the first two samples, with relatively high CaO (5.03 wt %) in JB1134 (top 1 cm), and
464 Na_2O (5.25 wt %) in JB1135 (2-5 cm) being the only notable differences from the other sample
465 abundances. Normalized K/Th values (Figure 9) range from 0.82 (JB1134, top 1 cm) to 0.86 (JB1138,
466 15-16 cm), which is significantly higher than the range of values (0.61-0.67) observed in the samples at
467 the core 2074 sample site. Limited variation of K/Th ratios is attributed to a lower degree of alteration in
468 samples at the core 39 sample site. The core 39 soil pit samples have the second-highest Th/U (Figure
469 10), K/Th, and Al/Ti ratios of the sample sites, which could indicate a higher degree of chemical
470 alteration than at the core 33 sample site. However, unlike the core 33 sample site, the core 39 sample
471 site is not in the path of any liquid water, and, therefore, its formation is likely dominated by sediment
472 mixing between multiple source rocks rather than processes associated with chemical alteration.

473

474 XRD analysis of core 39 soil pit samples (Table 5) shows an abundance of salts between samples
475 JB1135 (2-5 cm) and JB1136 (6-8 cm), supporting Everett Gibson's hypothesis of a salt layer in this
476 depth range. Thenardite is the dominant salt in these two samples. Gypsum is reported in JB1137 (10-12
477 cm), and anhydrite and halite are reported in JB1135 (2-5 cm). Low quartz abundances in JB1135 (2-5
478 cm) and JB1136 (6-8 cm) are likely due to a dilution effect from the high salt content. Quartz abundance
479 is consistent in all other samples. Albite appears to be enriched in JB1138 (15-16 cm) and augite in
480 JB1134 (top 1 cm). JB1135 (2-5 cm) and JB1136 (6-8 cm) exhibit the two highest Na_2O values, which
481 seem to confirm the reports of thenardite. JB1134 (top 1 cm) exhibits the highest CaO, verifying the
482 report of epidote as measured by XRD.

483

484 Reflectance spectral analysis of core 39 soil pit samples (Figure 7) yields primarily quartz, feldspar, and
485 pyroxene. Spectral bands characteristic of gypsum near 2.0 and 2.5 μm (Bishop, 2019) are strongest in
486 the upper sediments (3-4 cm and 5-6 cm). Bands near 1.39, 1.93, and 2.19 μm are attributed to poorly
487 crystallized aluminosilicates like allophane and are strongest in the lower sediments. The presence of
488 allophane instead of crystalline clay minerals indicates limited soil maturity (Patel et al., 2015). An

additional band near 2.36 μm is due to an OH combination band in chlorite that is most consistent with Fe-rich chamosite (Bishop, 2019). This is a high-temperature phyllosilicate and likely part of the primary material rather than an alteration phase. Spectral features associated with quartz and feldspar are observed in the mid-IR spectral region (Figure 7b) and are detected by XRD. Notably, soil pit samples from Core 42, taken at a pond to the east, also exhibit allophane in approximately the same depth range, and chemical alteration was concluded to be the cause (Burton et al., 2023). Core 42 soil pit samples also bear mineralogically-diagnostic spectra suggestive of a chemically-altered clay-rich layer. Major and trace (REEs included) element enhancement reported by Burton et al. (2019), and Foerder (2020) support this conclusion. JB1137 (10-12 cm) also exhibits major and trace element enhancement along with spectra diagnostic of a clay-rich layer similar to that of Core 42 soil pit samples (Burton et al., 2023).

JB1138 (15-16 cm) shows a drastic depletion in REE abundance compared to JB1137 (10-12 cm) slightly above it, suggesting the clay-rich layer is closer to JB1136 (6-8 cm) than to JB1138 (15-16 cm). This is supported by mineralogical observations made in the 5-8 cm range (Table 5). REE analysis (Figure 3) shows significant variation across samples. JB1135 (2-5 cm) exhibits the lowest values and JB1137 (10-12 cm) the highest. C1-chondrite normalized abundances (Taylor and McLennan, 1985) of La, Ce, and Nd increase steadily from JB1135 (2-5 cm), through JB1136 (6-8 cm), peak in JB1137 (10-12 cm), and decrease in JB1138 (15-16 cm), JB1135 (2-5 cm), and JB1136 (6-8 cm). These elements are, however, depleted in nearly all elements, particularly Sm, Eu, and Gd, relative to samples from the core 2074 and 33 sample sites. Sediment mixing in the alluvial fan near the Core 39 sample site could be the reason for the chemical inconsistencies in the top 8-10 cm.

Conversely, the continuous cycling of REEs from a leaching zone near the surface to deeper parts of soil profiles could create an enriched REE reservoir in the subsurface (Nesbitt and Markovics, 1997). JB1137 (10-12 cm), a sample with a high abundance of REEs, could be the result of such a process. This would then suggest that chemical alteration is occurring near the surface and is cycling REEs downwards to depths where physical alteration dominates.

Soluble ion distribution throughout Core 39 (Table 4 and Figure 4c) shows the greatest variability with the highest relative abundances of both Na^+ and Cl^- at a depth of about 5 cm, indicating that NaCl is the

most prominent salt species. Ca^{2+} is less abundant compared to Na^{+}. The peak in Cl^{-} abundance at 5 cm depth correlates with observations by Patel et al. (2015) and Gibson et al. (1983).

Chemical Alteration of Don Juan Basin Samples

Major element abundances of soil samples can also provide insight into weathering processes if the provenance of soil components is similar for each core location. All soil pit samples exhibit comparable abundances of Fe_2O_3 between 3.34 and 5.24 wt % (see Table 2). However, starting from the center of DJP with the core 2074 sample site, both Al_2O_3 (5.74-11.9 wt %) and TiO_2 (0.28-2.19 wt %) abundances increase on average with distance from the pond, i.e., from Core 2074 to Core 39. Al_2O_3, TiO_2, and Fe_2O_3 abundances for the core 2074, 33, and 39 soil pit samples are applied and analyzed because of their relative insolubility and are compared in a ternary diagram in Figure 8. The points in the diagram come from the abundances in Table 2. The abundances of Al_2O_3, TiO_2, and Fe_2O_3 for each sample are summed and treated as 100 wt % for the diagram, and each sample's respective individual oxide abundance is treated as a fraction of the whole.

Data from the core 33 (150 m SW) and the core 39 sample sites (300 m SW) plot between Basement Granitoids and Ferrar Dolerite, with a trend towards Ferrar Dolerite. The increase in Al_2O_3 and decrease in TiO_2 abundances, starting at the core 39 sample site and ending at the core 2074 sample site, provide further evidence in support of an increasing chemical alteration gradient with proximity to DJP. Rare Earth Element concentrations, primarily for light REEs, depicted in Figure 3, show a clear relationship with proximity to DJP: the samples at the core 2074 sample site have the lowest abundance of La, Ce, and Nd, while the core 33 and core 39 soil pit samples exhibit increasing abundance. This trend further corroborates our hypothesis of an increasing chemical alteration gradient with proximity to DJP. Heavy REEs do not differ significantly across all the sample sites.

Table 5 compares mineralogical results from spectral analysis and XRD. Minerals are listed in order of abundance. Overall, there is a good correlation between spectral analysis and XRD results. Both reliably detected quartz in all samples, as well as pyroxene and silicate minerals (augite, mica, orthoclase, albite). Sulfate salts (anhydrite, gypsum, thenardite) are identified by XRD at depths that do not align

551 with spectral or chemical analyses in all cases. However, both analytical methods support a strong
552 decreasing gradient in the abundance of sulfate salts with distance from the center of DJP, further
553 strengthening our hypothesis of an increasing gradient of chemical alteration with proximity to DJP.
554 Total sulfur as measured by XRF supports this finding. It has been observed that in other core and
555 scooped samples across the region (Foerder, 2020; Burton et al., 2022), omitting the core 2074 sample
556 site, that a lens of sulfate salts notably persists, and in greatest abundance, between ~ 4-12 cm. This salt
557 lens serves as evidence for chemical alteration and is likely the result of a protective layer of sediment
558 preventing destabilization through physical alteration (e.g., wind, sublimation, evaporation). It is
559 important to note that XRD and reflectance spectral analysis specialize in measuring different properties.
560 XRD primarily focuses on identifying crystalline phases while reflectance spectroscopy focuses on
561 vibrations between chemical bonds. Because of this, both methods have specific minerals that generate
562 stronger or weaker signals that ultimately make a quantitative determination of mineral abundances
563 difficult. As a result, the data in Table 5 are strictly qualitative but are listed in the perceived order of
564 abundance.
565
566 McLeod et al. (2009) classify soils that are marginal to DJP as Salic Aquorthels. However, based on
567 results from Gibson et al. (1983), Patel et al. (2015), and results from this investigation, the designation
568 of Salic Aquorthel only applies to samples at the core 39 sample site, 300 m southwest of DJP, based on
569 anion distribution. Samples at the core 2074 and core 33 sample sites, importantly, do not have a salic
570 horizon with an upper boundary within 100 cm of the mineral soil surface. This may be the result of
571 aqueous inundation that only extended as far as the core 33 sample site, but not as far as the core 39
572 sample site. Analysis of soluble ions (Figure 4) corroborates this hypothesis, as a consistent abundance
573 of soluble ions Ca^{2+}, Na^{+}, and Cl^{-} are seen in samples from the core 2074 and 33 sample sites, while the
574 core 39 soil pit samples exhibit significantly greater variability of these ions. Similarly, $\delta^{34}S$ values of
575 sulfates in the samples from the core 2074 and 33 sites are comparable, while those at the core 39 site
576 are significantly lower (Szynkiewicz and Bishop, 2021).
577
578 The K/Th ratio of DJP core samples may be another useful parameter in assessing the extent of aqueous
579 alteration as K, Th, and their host minerals, behave differently in aqueous solutions due to the higher
580 solubility of K compared to Th. This raises the possibility that the K/Th ratio and the concentration of K
581 (ppm) can be used to assess the extent to which surface materials interacted with water, and therefore are

582 chemically altered (Taylor et al., 2006). In Figure 9, the K/Th ratio of DJP core samples, normalized to
583 an average terrestrial K/Th ratio of 2900 (Taylor et al., 2006), is shown as a function of K (ppm)
584 abundance. K/Th ratios of the local geologic constituents "MDV, Granitoids" (Palmer, 1987, 1990;
585 Ellery, 1989) and "MDV, Ferrar Dolerite" (Grapes et al., 1989; Morrison, 1995) are included for
586 comparison. Barton Peninsula Rocks and Soils (Lee et al., 2004) are included, as well, serving as
587 samples from a more chemically-altering environment. K abundances (on the x-axis) place the DJP core
588 samples at the lower end of the Basement Granitoids distribution and the higher end of the Ferrar
589 Dolerite distribution. The K/Th ratio of samples at the core 2074 sample site is high with respect to the
590 corresponding K abundances, whereas the samples from the core 33 and core 39 sample sites have K/Th
591 ratios and K abundances that fit the lower range of the Basement Granitoids well. This is supported by
592 the report of granitic patches (Winsor et al., 2020) found amongst a predominantly dolerite basin floor
593 (Peterson and Marsh, 2008). Analysis of abundances of elements such as K, Th, Fe, Ca, La, and Ce
594 show that our samples best align with the local and regional Ferrar dolerite deposit and the sampling
595 depth of our cores (< 30 cm) and the reported depth of the dolerite deposit (15-50 m at the most) support
596 this conclusion. Based on this, more than one primary constituent is likely undergoing alteration,
597 however, the Ferrar Dolerite deposit is the most likely in situ influence on the elemental makeup of our
598 samples.
599
600 As shown with other diagnostic measurements, a chemical and mineralogical gradient exists with
601 proximity to DJP, and such is the case for K/Th vs K (ppm). Lower values are measured closer to the
602 center of the pond (core 2074 sample site) and higher values are measured farther from the pond (core
603 39 sample site). The low K/Th vs. K (ppm) values exhibited by samples from the core 2074 sample site
604 are suggestive of past and/or present chemical alteration and that chemical alteration decreases in
605 intensity with distance from the pond. Interestingly, observed K/Th vs K (ppm) for samples at the core
606 2074 sample site exhibit a similar K (ppm) abundance to Ferrar Dolerite, yet have unexpectedly high
607 K/Th values, while samples from cores 33 and 39 sample sites trend away from core 2074 site samples
608 and Ferrar Dolerite, and better align with samples from a different environment altogether: Barton
609 Peninsula, King George Island. We include data from Barton Peninsula (Lee et al., 2004) because of the
610 region's geologically-similar basaltic andesite (Lee et al., 2004) to the dolerite floor of Don Juan Basin
611 (Peterson and Marsh, 2008). However, a distinct difference between the two is their respective
612 proximities to the coast and therefore regional/local humidities. Barton Peninsula sits directly on the

water and rarely experiences humidities below 70 % (Meteoblue 2020 Weather Archive) while Don Juan Basin is ~ 90 km inland and experiences annual humidities around 40-50 % (Doran et al., 2002; Dickson et al., 2013). A coastal environment with higher humidity is more prone to chemical alteration, while the opposite is usually true for an inland, desert environment like the MDV (e.g., Nichols, 2009). With Don Juan Basin samples continuing to show evidence of chemical alteration, the added comparison of rock and soil samples from Barton Peninsula provides us with an additional method by which to assess the degree of chemical alteration occurring in Don Juan Basin. Because K/Th vs K (ppm) values from the arid, inland samples better align with those from the more humid coastal samples, and the two environments exhibit similar primary geology, the case for in situ chemical alteration of the Don Juan Basin samples is strengthened.

Another diagnostic elemental ratio is Th/U due to the relative immobility of the two elements. Similarities in ionic size and bond structure allow for thorium and uranium to be chemically comparable and can explain why they tend to occur together in igneous rocks and hydrothermal ore deposits that form at high temperatures. However, at the surface, uranium is chemically more mobile. This is due to the limited stability of Th^{4+} chemical complexes that form in a natural environment, especially those with carbonate, and the distinct insolubility of Th^{4+} salts, compared with those of U^{4+} and U^{6+} at low temperatures (Mernagh and Miezitis, 2008). Th/U vs depth is shown in Figure 10. Results show that samples from the core 2074 sample site, in the center of DJP, have the lowest Th/U values while Th/U values increase outwards towards the core 33 and 39 sample sites, which are located 150 and 300 m to the southwest, respectively. This suggests a decrease in chemical alteration contributions with distance away from DJP.

The Chemical Index of Alteration (CIA) as proposed by Nesbitt and Young (1982) could support the proposed chemical alteration gradient. We discuss findings from our proposed correction to the CIA equation (detailed in Methods - Characterizing Sediment Alteration) where we assume a dilution effect, caused primarily by sulfate and chloride salts, can influence the final CIA value. Figure 11a shows the uncorrected CIA values plotted as a function of $Al_2O_3/TiO_{2\,(molar)}$ and Figure 11b shows the salt-corrected CIA_{Salt} values plotted as a function of $Al_2O_3/TiO_{2\,(molar)}$. Results for uncorrected CIA values as a function of $Al_2O_3/TiO_{2\,(molar)}$ show an increasing gradient with samples from the core 2074 sample site exhibiting the lowest CIA values (15 and 23) and samples from the core 33 sample site (34 to 40) and

core 39 sample site (36 to 48) exhibiting a higher range of values. A salt dilution effect may explain this unexpectedly inverted chemical alteration gradient. Aeolian sediment mixing of local geologic constituents, as well as aeolian salt input, could influence the CIA. However, CIA values of surface sediments throughout Wright Valley remain low and similar to those of the local parent rocks (Bishop et al., 2014; Foerder et al., 2020) and surface salts that are not under unique conditions, like those at DJP, would like destabilize under the extreme climatic conditions across the MDV. The effect of mass-wasting on the CIA would mainly impact the Core 39 sample site due to its proximity to the basin walls and a stream-incised rock glacier, enabling possible sediment entrainment and input.

Salt-corrected CIA_{Salt} values (see Methods - Characterizing Sediment Alteration) of JB1124 and JB1125 samples (core 2074 sample site) are ~100—indicating fully chemically-altered samples—and are likely the result of the highest reported total salt abundance (sum of salts reported by XRD) of all samples investigated. The corrected CIA_{Salt} values for samples at the core 33 sample site show significant alteration in most samples. Corrections are described as follows: CIA 38 to CIA_{Salt} 60 for JB1130 (3-4 cm); CIA 35 to CIA_{Salt} 100 for JB1131 (8-10 cm); and CIA 37 to CIA_{Salt} 82 for JB1132 (12-14 cm). A small correction of CIA 35 to CIA_{Salt} 47 is reported for surface sample JB1129 (0-1 cm) and is most likely due to its minor abundance of salts. The assumption that the sole source of SO_3 and Cl^- salts in our study is due to in-situ alteration at the sample core sites may be an oversimplification and salt sourcing from the DJP brine in permanently and temporarily inundated areas is likely. XRD analysis in Table 5 provides evidence that JB1124 and JB1125 display unaltered parent material, but this only serves as a qualitative assessment of their presence. An estimate would indicate that the abundance of unaltered parent materials is unlikely to surpass 20 % in these two samples. For core 33, which also exhibits evidence of historical aqueous inundation, a similar sourcing of salts is likely for samples JB1131 and JB1132. For these and other core 33 samples, it is likely that the unaltered parent material does exceed 20 %. As expected, CIA values from soil pit samples taken near core 39 are the least modified. For example, JB1135 (2-5 cm) and JB1136 (6-8 cm) are adjusted from CIA 31 to CIA_{Salt} 45 and from CIA 39 to CIA_{Salt} 62, respectively. After applying the salt-modified CIA equation, the chemical alteration gradient is reversed and aligns with the results from all other chemical alteration indicators in our investigation. This supports our hypothesis of intense chemical alteration at the center of DJP that decreases with distance while supporting the application of a salt-corrected CIA. The CIA_{Salt} values for soil pit samples taken near core 39 are likely

This is the peer-reviewed, final accepted version for American Mineralogist, published by the Mineralogical Society of America.
The published version is subject to change. Cite as Authors (Year) Title. American Mineralogist, in press.
DOI: https://doi.org/10.2138/am-2022-8779. http://www.minsocam.org/

675 # IMPLICATIONS FOR MARS

676

677 ## Analog Potential

678

679 The "analog approach" to planetary geology allows researchers to compare the four natural subsystems
680 on Earth that make up our geosphere, hydrosphere, atmosphere, and biosphere to those of other
681 planetary bodies. The MDV have long been considered one of the closest terrestrial analogs to the
682 martian environment due to climatic, geologic, and chemical similarities (Cameron et al., 1970;
683 Horowitz and Cameron, 1972; Morris et al., 1972; Gibson et al., 1983), although the MDV have a higher
684 Si level compared to Mars. These similarities have been used to model the geologic/geochemical
685 processes that may occur on Mars (Gibson et al., 1983; Wharton et al., 1989; Bishop et al., 2013, 2014a;
686 Dickson et al., 2013). Geochemical data from Gale Crater, Mars, have for some time implied the ancient
687 presence of aqueous environments at varying geospatial extents (e.g. Grotzinger et al., 2012, 2014,
688 2015; Vaniman et al., 2018; Vasavada, 2022) with recent studies (e.g., Liu et al., 2021) suggesting
689 small, acidic, pond-like bodies of water rather than several large, extensive bodies. If such a model of
690 Gale crater is correct, it strengthens the comparability of the two environments. The Spirit rover
691 investigated sulfate-rich outcrops at Gusev crater (e.g., Lane et al., 2008; Yen et al., 2008) and the
692 Opportunity rover investigated sulfate-rich outcrops at Meridiani Planum, including the Burns formation
693 thought to contain gypsum (e.g., Squyres et al, 2004; Arvidson et al., 2015). Other sites on Mars
694 containing elevated sulfate abundances based on orbital data include the many chasma in the Valles
695 Marineris region, Aram Chaos, and Olympia Undae near the north polar region (e.g., Murchie et al.,
696 2019), but these sites have not yet been visited by a rover to obtain in situ chemical and mineralogical
697 data.

698

699 ## Sulfur

700

701 Sources of sulfur in the MDV (Claridge and Campbell, 1968, 1977) and on Mars (Settle, 1979; Farquhar
702 et al., 2000; Farquhar et al., 2007) are both considered to be primarily atmospheric, though, in the case
703 of the MDV, less so than previously thought (Szynkiewicz and Bishop, 2021). Atmospheric sulfur in
704 MDV samples is largely regarded as originating in aqueous aerosols from the Ross Sea/McMurdo
705 Sound, eventually settling and forming sulfate minerals such as gypsum (Claridge and Campbell, 1968,

706 1977). Microbial sulfate reduction is supported in the MDV, and could be occurring in deeper sediments
707 given that the brine underlying Don Juan Pond is depleted in dissolved sulfate even at depths of 75 m
708 (Szynkiewicz and Bishop, 2021) compared to elevated calcium and chloride concentrations (Harris,
709 1981), however, this is not the leading hypothesis. Alternatively, sulfur in Mars rover samples is
710 believed to originate in the martian mantle and to have been expelled into the atmosphere during
711 volcanic outgassing (Jones, 1989; Farquhar et al., 2000b; King et al., 2004; Franz et al., 2014a;). The
712 outgassed SO_2 is assumed to have undergone photochemical conversion to H_2SO_4, forming surficial
713 sulfate minerals (Settle, 1979; Farquhar et al., 2000; Farquhar et al., 2007). Though atmospheric
714 contribution is presumed to be an important source of sulfur in the MDV and on Mars, in situ chemical
715 weathering, as a result of interaction between DJP's underlying aquifer and dolerite bedrock (Harris,
716 1981; Harris and Cartwright, 1981), is likely a contributing factor (Szynkiewicz and Bishop, 2021).
717
718 Martian sulfur enrichment has been suggested to represent evaporites deposited at a time when there was
719 a more active hydrological cycle on the surface of the planet (e.g., Golombek et al., 1999; McLennan et
720 al., 2005; Grotzinger et al., 2014, 2015) and it is thought that MDV sediments enriched in evaporites
721 have sulfur abundances similar to those found on Mars (e.g., Gibson, 1983; Wentworth et al., 2005;
722 Head and Marchant, 2014). The average sulfate abundance of martian rocks measured at Gale crater by
723 the Curiosity rover is ~ 4.8 wt % and the average soil sulfate abundance is ~ 8.6 wt % (e.g., Vaniman et
724 al., 2014; McSween, 2015; Berger et al., 2016; Thompson et al., 2016a, 2016b; Treiman et al., 2016).
725 Notably, calculated sulfate abundances from DJP samples near core 2074 are ~ 14 wt % (JB1124, 1-2
726 cm) and ~ 9 wt % (JB1125, 8-10 cm). Sample JB1131 from the core 33 site (8-10 cm) reports ~ 4 wt %
727 and all samples from the core 39 site report <1 wt %.
728
729 As for martian mineralogy, Curiosity has analyzed numerous targets from different formations inside
730 Gale crater using the ChemMin X-Ray Diffraction instrument (Nochan et al., 2014; Morris et al. 2016;
731 Treiman et al., 2016; Vaniman et al. 2014; Rampe et al. 2017; Bristow et al. 2017; Yen et al., 2017).
732 Examples of formations so far visited by Curiosity include Yellowknife Bay, Murray, Stimson, and
733 Kimberly. Every target within each martian formation contained largely basaltic detritus and in some
734 cases an X-ray amorphous component. All targets contained sulfate, with gypsum, anhydrite, and
735 bassanite as the most common crystalline salt species. The majority of samples analyzed by CheMin
736 were targeted to emphasize matrix mineralogy, although light-toned veinlets and/or nodules were

unavoidable in some drill holes (Vaniman et al., 2018). Samples therein are compared to those collected in and around Don Juan Basin, Antarctica. Yellowknife Bay targets contain Ca-sulfates such as anhydrite and bassanite (Vaniman et al., 2013; Ming et al., 2014; Vaniman et al., 2018); this was further confirmed by ChemCam (Nahcon et al., 2014) and the APXS instrument (McLennnan et al., 2013). Targets analyzed from the Murray Formation recorded between 8 and 35 wt % anhydrite, and between 3 and 18.5 wt % gypsum (Vaniman et al. 2014, 2018; Morris et al. 2016; Bristow et al. 2017; Rampe et al. 2017; NASA Planetary Data System; Astrobiology Habitable Environments Database). The Murray Formation notably exhibits sequences of thick and thin laminated mudstone (Rampe et al., 2020) consistent with fluvio-lacustrine deposition (e.g., Fedo et al., 2018; Stack et al., 2018; Tu et al., 2021). The Stimson Formation had fractures and matrices analyzed, notably yielding 3-4.5 wt % anhydrite in the fracture samples while the matrix samples contained <1 wt % of anhydrite and/or bassanite (Yen et al., 2017; Vaniman et al., 2018). It is possible that anhydrite could have formed by dehydration of gypsum at Gale crater, but widespread anhydrite in sedimentary rocks is more likely formed by growth from solution (Vaniman et al., 2018). In a dilute solution, anhydrite generally forms above ~ 40 to 60 °C (e.g., Hardie 1967; Van Driessche et al., 2017). However, in a concentrated brine, anhydrite can form at temperatures as low as 18 °C, and as low as ~ 0 °C in residual solution for a modeled brine with <4 % remaining fluid at Meridiani Planum (Marion et al. 2009, 2016). Groundwater dynamics and matrix mineralogy have been shown to complicate the outcome: in experiments with $CaCl_2$ brine and K-jarosite matrix–a sulfate mineral ($[KFe^{3+}_3(SO_4)_2(OH)_6]$) found in much greater abundance on Mars than on Earth—Miller et al., 2017, reports the precipitation of only gypsum in static systems, but gypsum and anhydrite in flowing systems. Furthermore, Miller et al., 2017, demonstrated that anhydrite can also form at low temperatures from jarosite alteration in $CaCl_2$ brines without a pre-existing gypsum phase if there is groundwater flow.

As with Mars, Don Juan Basin remains an extremely cold, dry, and igneous environment, with the added presence of highly saline, stable surface water. The report of widespread martian jarosite (Klingelhöfer et al., 2004; Farrand et al., 2009; Weitz et al., 2015; Rampe et al., 2017), gypsum, and anhydrite (Nochan et al., 2014; Morris et al. 2016; Treiman et al., 2016; Vaniman et al. 2014; Rampe et al. 2017; Bristow et al. 2017; Yen et al., 2017), and the aqueous conditions they require to form, has been interpreted as a sign that transient, chemically-altering fluids were active on Mars (Elwood-Madden et al., 2009, Vaniman et al., 2018). Though lacking jarosite, sulfate mineralogy in Don Juan Basin

768 sediments is predominantly expressed as aqueously-derived anhydrite and gypsum with comparable
769 abundances to those measured by the Curiosity rover. Our measurements from DJP show that anhydrite
770 can form under low-temperature conditions, providing relevancy to Gale crater when deliberating on
771 past climate. Additionally, many of the gypsum deposits measured by CheMin were reported in depth
772 ranges of 2-6 cm, likely due to a protective layer of surface sediment helping maintain mineral stability
773 (Vaniman et al., 2018). We believe this to also be the case for Don Juan Basin samples with gypsum
774 measured at similar depth ranges.
775
776 **Sediment Alteration on Mars**
777
778 Environmental temperatures and grain size have been shown to influence the Chemical Index of
779 Alteration in terrestrial and martian samples (Thorpe et al., 2021). Our observations indicate that in the
780 presence of salts, the CIA_{Salt} correction (developed in Methods - Characterizing Sediment Alteration)
781 needs to be applied. Figure 11c compares uncorrected and salt-corrected CIA values for Don Juan Basin
782 samples at the core 2074 sample site to rock and soil samples obtained by the Curiosity rover as a
783 function of the ratio $Al_2O_3/TiO_{2\ (molar)}$ (e.g., Vaniman et al., 2014; McSween, 2015; Berger et al., 2016;
784 Thompson et al., 2016a, 2016b; Treiman et al., 2016). Several studies (e.g., McLennan et al., 2014;
785 Hurowitz et al., 2017; Siebach et al., 2017, 2018, 2020; Mangold et al., 2019) have applied the CIA
786 equation (Nesbitt and Young, 1982) to samples from martian formations, such as Yellowknife Bay,
787 Murray, and Bradbury. They have largely reported low CIA values.
788
789 Correcting for salt abundances, most Curiosity rock and soil samples show higher CIA_{Salt} values (as high
790 as ~77), accounting for a $CaCl_2$ and $CaSO_4^{2-}$ dilution effect and suggesting that there are Ca-chloride/-
791 sulfate salts on Mars, thus, supporting the likelihood of past or present chemical alteration on Mars.
792 Both CIA and corrected CIA_{Salt} values for Curiosity rock and soil samples are within 1 wt % of each
793 other despite the soils containing sulfate abundances nearly twofold. The CIA_{Salt} best accounts for $CaCl_2$
794 and $(Ca, Na_2, K_2) \cdot SO_4^{2-}$ in samples from martian and Antarctic surfaces. The scarcity of Na^+ and K^+,
795 and the relative abundance of Ca^{2+} (Tosca et al., 2004; Tosca and McLennan, 2006) at the martian
796 surface means that CIA_{Salt} only modifies CaO abundance for the presence of $CaCl_2$ and $CaSO_4^{2-}$–not
797 $(Na_2, K_2) \cdot SO_4^{2-}$. Curiosity CIAs for soil samples that exhibit approximately twice the sulfate abundance
798 of the rocks may be underestimated by the CIA_{Salt} corrections. $MgSO_4$ salt (kieserite) has been recorded

at several sites on the martian surface, with the highest abundances in the Valles Marineris region (Murchie et al., 2009), but is not accounted for in the original or our CIA_{Salt} equation. This may lead to an underestimation of salt dilution and possibly an underestimation of the extent of chemical alteration that is taking place on Mars. Additional obstacles in the use of the CIA on salty samples include cations binding to more than just sulfate, and sulfate binding to more than just one cation.

SUMMARY AND CONCLUSIONS

Elemental, spectral, and mineralogical analyses conducted on samples from the soil pit samples taken near cores 2074, 33, and 39 from Don Juan Basin in the MDV, Antarctica support an increasing chemical alteration gradient from the center of the pond outwards. Our results show that the core 2074 sample site, located in the center of DJP, exhibits the highest abundance of salts (primarily anhydrite and gypsum), the lowest relative abundance of major elements, the lowest elemental ratios of K/Th and Th/U, and the highest salt-corrected CIA_{Salt} values at all sample depths.

Therefore, we conclude that the soil pit samples at the core 2074 sample site, located in the center of DJP, display the greatest degree of chemical alteration. Samples from the core 33 sample site, 150 m southwest of the core 2074 sample site, exhibit a lower abundance of salts (primarily observed between 8-12 cm), elevated abundances of major elements, elevated K/Th and Th/U ratios, and lower CIA_{Salt} values, indicating that the soil pit samples taken near core 33 have a lower degree of chemical alteration than the samples from the core 2074 sample site. Additionally, based on the definition of Salic Aquorthel (McLeod et al., 2009) and anion analysis, DJP may once have extended as far as the core 33 sample site. Lastly, the core 39 sample site, 300 m southwest of the core 2074 sample site, records the lowest abundance of salts (observed between 4-10 cm), the highest relative abundance of major elements and K/Th and Th/U ratios, and the lowest CIA_{Salt} values. Effects of chemical alteration are found in layers where elemental enrichment within the sediment column is observed at depths where physical alteration is limited. Samples from the core 39 sample site exhibit the lowest degree of chemical alteration in the Don Juan Basin sites investigated. Important to this conclusion is that core 39 samples and the adjacent soil pit samples qualify as Salic Aquorthels, which shows that the influence of DJP fluids reached as far as the core 33 sample site, but not as far as the core 39 sample site. The observed decreasing gradient of chemical alteration with distance from DJP, the different soil

classification of samples at the core 39 sample site, soluble ion distribution, and δ^{34}S values of sulfates suggest a closer relationship between samples taken near cores 33 and 2074, supporting the model of a once larger, more extensive, and dilute DJP. A higher concentration of salts at the center of the pond, potentially because of a receding shoreline over as much as 2 million years (Calkin et al., 1970), in tandem with evaporative concentration, bolsters this interpretation.

Bishop et al. (2014a) compared normalized K/Th ratios and the Chemical Index of Alteration to evaluate relationships among Dry Valley sediments at several surface locations in Wright and Taylor valleys with low S and Cl abundances, concluding that physical alteration dominates across the regions of investigation. Comparison of their MDV elemental data to trends observed in martian meteorites and at the surface of Mars at Gusev crater and Meridiani Planum suggested that physical alteration has played a greater role than chemical alteration. However, our investigation suggests that martian data are highly dependent on sulfur and chlorine content, which can skew the CIA when combined with major elements of the equation to form sulfate or chloride salts. Specific to Mars, our study supports the utility of a Ca-chloride/sulfate-modified CIA_{Salt} equation to correct for what is believed to be a salt dilution effect and underrepresentation of actual chemical alteration.

The cold and dry conditions, igneous geology, sulfate source, deposition, abundance, and species currently present in Don Juan Basin microenvironments (namely adjacent to cores 2074 and 33) appear strikingly comparable to a host of martian microenvironments (rover sample sites). Additionally, results from our CIA and our CIA_{Salt} analysis suggest that the corrected CIA_{Salt} equation can be applied and utilized beyond Earth to assess the extent of chemical alteration. The similarities demonstrate a promising terrestrial analogy between microenvironments of the MDV and Mars.

Acknowledgments: Support was provided by the Hawai‘i Institute of Geophysics and Planetology, the Department of Earth Sciences at the University of Hawai‘i at Mānoa, and the SETI Institute. We thank D. Mader (Univ. Vienna) for help with the trace element analyses, and the Mars Science Lab science team for collecting and archiving the data from Gale crater. We are grateful to L. McHenry for helpful comments and editorial handling.

862 **References**:

863

864 Anderton P. H. (1976) Hydrological Research, Annual Report #37, Dry Valleys, Antarctica, 1973-74.
865 Christchurch: New Zealand Ministry of Works and Development, 14.

866

867 Arvidson, R. E., Bell J. F., Catalano J. G., Clark B. C., Fox V. K., Gellert R., Grotzinger J. P., Guinness
868 E. A., Herkenhoff K. E., Knoll A. H., Lapotre M. G. A., McLennan S. M., Ming D. W., Morris
869 R. V., Murchie S. L., Powell K. E., Smith M. D., Squyres S. W., Wolff M. J., and Wray J. J.
870 (2015) Mars Reconnaissance Orbiter and Opportunity observations of the Burns formation:
871 Crater hopping at Meridiani Planum. Journal of Geophysical Research: Planets, 120,
872 2014JE004686.

873

874 Astrobiology Habitable Environments Database,
875 https://odr.io/CheMin#/search/display/84/eyJkdF9pZCI6IjQzIn0/1 (Accessed June 2022).

876

877 Banham, S. G., Gupta, S., Rubin, D. M., Watkins, J. A., Sumner, D. Y., Edgett, K. S., Grotzinger, J. P.,
878 Lewis, K. W., Edgar, L. A., Stack-Morgan, K. M., Barnes, R., Bell, J. F., Day, M. D., Ewing, R.
879 C., Lapotre, M. G., Stein, N. T., Rivera-Hernandez, F. and Vasavada, A. R. (2018), Ancient
880 Martian aeolian processes and paleomorphology reconstructed from the Stimson formation on
881 the lower slope of Aeolis Mons, Gale crater, Mars. Sedimentology, 65, 993-1042.

882

883 Bao H., Campbell D.A., Bockheim J.G., and Thiemens M. H. (2000) Origins of sulphate in Antarctic
884 dry-valley soils as deduced from anomalous ^{17}O compositions. Nature, 407, 499-502.

885

886 Berger J. A., Schmidt M. E., Gellert R., Campbell J. L., King P. L., Flemming R. L., Ming D. W., Clark
887 B. C., Pradler I., VanBommel S. J. V., Minitti M. E., Fairén A. G., Boyd N. I., Thompson L.
888 M., Perrett G. M., Elliott B. E., and Desouza E. (2016) A global mars dust composition refined
889 by the Alpha Particle X-ray Spectrometer in Gale Crater. Geophysical Research Letters, 43, 67-
890 75.

891

892 Bishop J. L., Koeberl C., Kralik, C., Froeschl H., Englert P. A. J., Andersen D. H., Pieters C. M., and
893 Wharton R. A. (1996) Reflectance spectroscopy and geochemical analyses of Lake Hoare
894 sediments, Antarctica. Geochimica Cosmochimica Acta, 60, 765-785.
895
896 Bishop J. L., Lougear A., Newton J., Doran P. T., Froeschl H., Trautwein A. X., Körner W., and
897 Koeberl C. (2001) Mineralogical and geochemical analyses of Antarctic sediments: a reflectance
898 and Mössbauer spectroscopy study with applications for remote sensing on Mars. Geochimica
899 Cosmochimica Acta, 65, 2875-2897.
900
901 Bishop J. L., Anglen B. L., Pratt L. M., Edwards H. G. M., Des Marais D. J., and Doran P. T. (2003) A
902 spectroscopy and isotope study of sediments from the Antarctic Dry Valleys as analogs for
903 potential paleolakes on Mars. International Journal of Astrobiology, 2, 273-287.
904
905 Bishop J. L., Franz H., Goetz W., Blake D., Freissinet C., Steininger H., Goesmann F., Brinckerhoff
906 W., Getty S., Pinnick V., Mahaffy P., and Dyar M. (2013) Coordinated analyses of Antarctic
907 sediments as Mars analog materials using reflectance spectroscopy and current flight-like
908 instruments for CheMin, SAM and MOMA. Icarus, 224, 309-325.
909
910 Bishop J. L., Englert P. A. J., Patel S. N., Tirsch D., Roy A. J., Koeberl C., Böttger U., Hanke F., and
911 Jaumann R. (2014a) Mineralogical analyses of surface sediments in the Antarctic Dry Valleys:
912 Coordinated analyses of Raman spectra, reflectance spectra and elemental abundances.
913 Philosophical Transactions of the Royal Society, A, 372, 20140198, 1-26.
914 Bishop, J.L., Lane M.D., Dyar M.D., King S.J., Brown A.J., and Swayze G. (2014b) Spectral properties
915 of Ca-sulfates: Gypsum, bassanite and anhydrite. American Mineralogist, 99, 2105-2115.
916
917 Bishop J. L. (2019) Chapter 4: Visible and near-infrared reflectance spectroscopy of geologic materials,
918 in: Bishop J. L., Bell III J. F., Moersch J. E. (Eds.), Remote Compositional Analysis: Techniques
919 for Understanding Spectroscopy, Mineralogy, and Geochemistry of Planetary Surfaces.
920 Cambridge University Press, Cambridge, U.K., 68-101.
921

Blake D. F., Morris R.V., Kocurek G., Morrison S.M., Downs R.T., Bish D., Ming D.W., Edgett K.S., Rubin D., Goetz W., Madsen M.B., Sullivan R., Gellert R., Campbell I., Treiman A.H., McLennan S.M., Yen A.S., Grotzinger J., Vaniman D.T., Chipera S.J., Achilles C.N., Rampe E.B., Sumner D., Meslin P.-Y., Maurice S., Forni, O., Gasnault O., Fisk M., Schmidt M., Mahaffy P., Leshin L.A., Glavin D., Steele A., Freissinet C., Navarro-González R., Yingst R.A., Kah L.C., Bridges N., Lewis K.W., Bristow T.F., Farmer J.D., Crisp J.A., Stolper E.M., Des Marais D.J., Sarrazin P., and the MSL Science Team (2013) Curiosity at Gale Crater, Mars: Characterization and analysis of the Rocknest sand shadow. Science, 341, No. 6153, 1239505.1-1239505.7.

Bristow, T. F., Blake, D. F., Vaniman, D. T., Chipera, S. J., Rampe, E. B., Grotzinger, J. P., McAdam, A. C., Ming, D. W., Morrison, S. M., Yen, A. S., Morris R. V., and Des Marais J. V. (2017) Surveying clay mineral diversity in the Murray Formation, Gale crater, Mars. 48th Lunar and Planetary Science, Abstract no. 2462.

Bull C. (1966) Climatological observations in ice-free areas of southern Victoria Land, Antarctica. In: Rubin M. J. (Ed.) Studies in Antarctic Meteorology, 9, American Geophysical Union, Antarctic Research Series, 177-194.

Burton Z. F. M., Bishop J. L., Englert P. A. J, Koeberl C., Gibson E. K. (2019) Salts and Clays Beneath Surface Sediments in Antarctica Provide Clues to Weathering and Geochemistry on Mars. 50th Lunar and Planetary Science Conference, Abstract no. 2132.

Burton Z. F. M., Bishop J. L., Englert P. A. J., Szynkiewicz A., Koeberl C., Dera P., McKenzie W., and Gibson E. K. (2022) A shallow salt pond analog for aqueous alteration on ancient Mars: Spectroscopy, mineralogy, and geochemistry of sediments from Antarctica's Dry Valleys. American Mineralogist, In Press.

Calkin P. E., Behling R. E., and Bull C. (1970) Glacial history of Wright Valley, southern Victoria Land, Antarctica. Antarctic Journal of the United States, 5, 22-27.

953 Cameron R. E., King J., and David C. M. (1970) Microbiology, ecology, and microclimatology of soil
954 sites in Dry Valleys of Southern Victoria Land, Antarctica. Antarctic Ecology, 2, 702-716,
955 Holdgate M. W. (Ed.), New York, NY: Academic Press.
956
957 Chinn T. (1976) Hydrological Research Report, Dry Valleys, Antarctica, 1974-75. Christchurch: New
958 Zealand Ministry of Works and Development, 45.
959
960 Chinn, T. J. (1993) Physical hydrology of the dry valley lakes. In: Green, W. J., and Friedman, E. I.
961 (eds.) Physical and biogeochemical processes in Antarctic lakes. Washington DC: American
962 Geophysical Union Antarctic Research Series, 1-51.
963
964 Claridge G. G. C. and Campbell I. B., (1968) Origin of nitrate deposits. Nature, 217, 428-430.
965
966 Claridge G. G. C. and Campbell I. B. (1977) The salts in Antarctic soils, their distribution and
967 relationship to soil processes. Soil Science, 123, 377-384.
968
969 Clark B. C. (1993) Geochemical components in Martian soil. Geochimica et Cosmochimica Acta 57,
970 4575-4581.
971 Clark B. C. and Van Hart D. C. (1980) The salts of Mars. Icarus, 45, 370-378.
972
973 Cullers R. L. and Graf J. (1984) Rare earth elements in igneous rocks of the continental crust:
974 intermediate and silicic rocks, ore petrogenesis. Rare-Earth Geochemistry, Henderson, P. (Ed.),
975 Elsevier, Amsterdam, 275-312.
976
977 Dickson J., Head J., Levy J., and Marchant D. R. (2013) Don Juan Pond, Antarctica: Near-surface
978 $CaCl_2$-brine feeding Earth's most saline lake and implications for Mars. Scientific Reports, 3,
979 Article No. 1166.
980
981 Doran P. T., Wharton Jr. R. A., and Lyons W. B. (1994) Paleolimnology of the McMurdo Dry Valleys,
982 Antarctica. Journal of Paleolimnology, 10, 85-114.

Doran P. T., McKay C. P., Clow G. D., Dana G. L., Fountain A. G., Nylen T., and Lyons W. B. (2002) Climate and surface heat balance in an Antarctic dry valley. New Zealand Journal of Science, 14, 245-251.

Ellery S. G. (1989) Lower Wright geology, Unpublished M.Sc. thesis, lodged in the Library, University of Otago, New Zealand.

Elwood Madden M. E., Madden A. S., and Rimstidt J. D. (2009) How long was Meridiani Planum wet? Applying a jarosite stopwatch to determine the duration of aqueous diagenesis. Geology, 37, 635-638.

Farrand W. H., Glotch T. D., Rice J. W. Jr, Hurowitz J. A., and Swayze G. A. (2009) Discovery of jarosite within the Mawrth Vallis region of Mars: implications for the geologic history of the region. Icarus, 204, 478-488.

Farquhar J., Savarino J., Jackson, T. L., and Thiemans M. H. (2000) Evidence of atmospheric sulphur in the martian regolith from sulphur isotopes in meteorites. Nature, 404, 50-52.

Farquhar J., Kim S. T., and Masterson A. (2007) Implications from sulfur isotopes of the Nakhla meteorite for the origin of sulfate on Mars. Earth and Planetary Science Letters, 264, 1-2, 1-8.

Fedo C. M., Nesbitt H. H., and Young G. M. (1995) Unraveling the effects of potassium metasomatism in sedimentary rocks and paleosols, with implications for paleo-weathering conditions and provenance. Geology, 23, 921-924.

Fedo C. M., Grotzinger J. P., Gupta S., Fraeman A., Edgar L., Edgett K., Stein N., Rivera-Hernandez F., Lewis K., Stack K. M., House C., Rubin D., and Vasavada A. (2018) Sedimentology and stratigraphy of the Murray formation, Gale crater, Mars. 49th Lunar and Planetary Science Conference, Abstract no. 2078.

Ferrar H. T. (1907) Report on the Field Geology of the Region Explored During the Discovery Antarctic Expedition, 1901-1904: National Antarctic Expedition, British Museum (Natural History), 1, 100.

Foerder A. B. (2020) Chemical Alteration and Soil Provenance of Polar Desert Sediments from the McMurdo Dry Valleys, Antarctica: An Analog for Alteration Processes on Mars, Master's Thesis, the University of Hawai'i at Mānoa, 1-312.

Franz H., Kim S. T., Farquhar J., Day J., Economos R., McKeegan K., Schmitt A., Irving A., and Dottin III J. (2014) Isotopic links between atmospheric chemistry and the deep sulphur cycle on Mars. Nature, 508, 364-368.

Gellert R. and Yen A. S. (2019) Chapter 28: Elemental Analyses of Mars from Rovers Using the Alpha-Particle X-Ray Spectrometer. In Remote Compositional Analysis: Techniques for Understanding Spectroscopy, Mineralogy, and Geochemistry of Planetary Surfaces (eds. J. L. Bishop, J. F. Bell III and J. E. Moersch). Cambridge University Press, Cambridge, UK. pp. 555-572.

Gibson E. K., Wentworth S. J., and McKay D. S. (1983) Chemical weathering and diagenesis of a cold desert soil from Wright Valley, Antarctica: An analog of martian weathering processes. Journal of Geophysical Research, 88, 912-928.

Golombek, M. P., Anderson R., Barnes J., Bell, J. F. Bridges N., Britt D., Brückner J., & Cook R. A., Crisp D., Crisp J. A., Economou T., Folkner W., Greeley R., Haberle R., Hargraves R. B., Harris J. A., Haldemann A., Herkenhoff K., Hviid S. F., and Wilson G. R. (1999) Overview of the Mars Pathfinder Mission: Launch through Landing, Surface Operations, Data Sets, and Science Results. Journal of Geophysical Research, 104, 8523-8554.

Grapes R., Gamble J., and Palmer P. (1989) Basal dolerite boulders. In: Barrett P.J . (Ed.), Antarctic Cenozoic history from CIROS-1 drillhole, McMurdo Sound. Department of Scientific and Industrial Research Bulletin, 245, 169-174.

Grindley, G. W. and Warren G. (1964) Stratigraphic Nomenclature and Correlation in the Western Ross Sea Region. Antarctic Geology, Adie R. J. (Ed.) Amsterdam, North Holland Publishing Company, and John Wiley and Sons, New York. 315-333.

Grotzinger J. P., Sumner D. Y., Kah L.C., Stack K., Gupta S., Edgar L., Rubin D., Lewis K., Schieber J., Mangold N., Milliken R., Conrad P.G., Des Marais D., Farmer J., Siebach K. L., Calef F 3rd., Hurowitz J., McLennan S. M., Ming D., Vaniman D., Crisp J., Vasavada A., Edgett K. S., Malin M., Blake D., Gellert R., Mahaffy P., Wiens R. C., Maurice S., Grant J. A., Wilson S., Anderson R. C., Beegle L., Arvidson R., Hallet B., Sletten R. S., Rice M., Bell J 3rd., Griffes J., Ehlmann B., Anderson R. B., Bristow T. F., Dietrich W. E., Dromart G., Eigenbrode J., Fraeman A., Hardgrove C., Herkenhoff K., Jandura L., Kocurek G., Lee S., Leshin L. A., Leveille R., Limonadi D., Maki J., McCloskey S., Meyer M., Minitti M., Newsom H., Oehler D., Okon A., Palucis M., Parker T., Rowland S., Schmidt M., Squyres S., Steele A., Stolper E., Summons R., Treiman A., Williams R., Yingst A., and the MSL Science Team (2014) A habitable fluvio-lacustrine environment at Yellowknife Bay, Gale crater, Mars. Science, 343 (6169), 1242777.1-1242777.14

Grotzinger J. P, Gupta S., Malin M. C., Rubin D. M., Schieber J., Siebach K. L., Sumner D. Y., Stack K. M., Vasavada A., Arvidson R. E., Calef F. 3rd., Edgar L., Fischer W. F., Grant J. A., Griffes J., Kah L. C., Lamb M. P., Lewis K. W., Mangold N., Minitti M. E., Palucis M., Rice M., Williams R. M., Yingst R. A., Blake D., Blaney D., Conrad P., Crisp J., Dietrich W.E., Dromart G., Edgett K. S., Ewing R. C., Gellert R., Hurowitz J. A., Kocurek G., Mahaffy P., McBride M. J., McLennan S. M., Mischna M., Ming D., Milliken R., Newsom H., Oehler D., Parker T. J., Vaniman D., Wiens R. C., and Wilson S. A. (2015). Deposition, exhumation, and paleoclimate of an ancient lake deposit, Gale crater, Mars. Science, 350 (6257), aac7575.1- aac7575.12.

Gunn B. M., and Warren G. (1962) Geology of Victoria Land between the Mawson and Mulock Glaciers, Antarctica: New Zealand Geological Survey Bulletin, 71, 1–157.

Hall B. L., Denton G. H., Lux D. R., and Schluchter C. (1997). Pliocene Paleoenvironment and Antarctic Ice Sheet Behavior: Evidence from Wright Valley. Journal of Geology, 105, 285-294.

Hardie L.A. (1967) The gypsum-anhydrite equilibrium at one atmosphere pressure. American Mineralogist, 52, 171-200.

Harnois, L., 1988, The CIW index: a new Chemical Index of Weathering, Sedimentary Geology, 55, 3-4, 319-322.

Harrington, H. J., 1958. Nomenclature of rock units in the Ross Sea region, Antarctica: Nature, 182 (4631), 290.

Harris H. J. H. and Cartwright K. (1981) Hydrogeology of the Dry Valley Region, Antarctica. In Dry Valley Drilling Project, 33, McGinnis L. D. (Ed.), American Geophysical Union, Washington D.C., 161-184.

Harris H. J. H. (1981) Hydrology and Hydrogeochemistry of the South Fork, Wright Valley, Southern Victoria Land, Antarctica. Doctoral Thesis, the University of Illinois at Urbana-Champaign, Department of Geology, 1-341.

Harris H. J. H. and Cartwright K., Torii T. (1979) Dynamic chemical equilibrium in a polar desert pond: A sensitive index of meteorological cycles. Science, 204, 301-303.

Hassinger J. M., and Mayewski P. A. (1983) Morphology and dynamics of the rock glaciers in Southern Victoria Land, Antarctica. Arctic Alpine Research, 15, 351-368.

Hastings S. J., Luchessa S. A., Oechel H. C., and Tenhunen J. D. (1989) Standing biomass and production in water drainages of the foothills of the Philip Smith Mountains, Alaska. Holarctic Ecology, 12, 304-311.

Head J. H., Marchant D. R., Dickson J. L., Levy J. S., and Morgan G. A. (2007) Slope streaks in the Antarctic Dry Valleys: Characteristics, candidate formation mechanisms, and implications for slope streak formation in the martian environment. 38th Lunar and Planetary Science Conference, Abstract no. 1935.

Head J., and Marchant D. (2014). The climate history of early Mars: Insights from the Antarctic McMurdo Dry Valleys hydrologic system. Antarctic Science, 26, 774-800.

Horowitz N. H. and Cameron R. E. S. H. J. (1972) Microbiology of the dry valleys of Antarctica. Science, 176, 242-245.

Hurowitz J. A., McLennan S. M., Tosca N. J., Arvidson R. E., Michalski J. R., Ming D. W., Schröder C., and Squyres S. W. (2006) In situ and experimental evidence for acidic weathering of rocks and soils on Mars. Journal of Geophysical Research: Planets, 111(2) E02S19.

Hurowitz J. A., Grotzinger J. P., Fischer W. W., McLennan S. M., Milliken R. E., Stein N., Vasavada A., Blake D. F., Dehouck E., Eigenbrode J. L., Fairén A. G., Frydenvang J., Gellert R., Grant J. A., Gupta S., Herkenhoff K. E., Ming D. W., Rampe E. B., Schmidt M. E., Siebach K. L., Stack-Morgan K., Sumner D. Y., and Wiens R. C. (2017) Redox stratification of an ancient lake in Gale crater, Mars. Science, 356 (6341), Art. no. eaah6849, 1-10.

Jagoutz E., Palme H., Baddenhausen H., Blum K., Cendales M., Dreibus G., Spettel B., Lorenz V., and Wänke H. (1979) The abundances of major, minor, and trace elements in the Earth's mantle as derived from primitive ultramafic nodules. Proceedings of the 10th Lunar Planetary Science Conference, 2031-2050.

Jones J. H. (1989) Isotopic relationships among the shergottites, the nakhlites, and Chassigny. Lunar and Planetary Institute, Houston. Proceedings of the 19th Lunar and Planetary Science Conference, 465-474.

King P. L., Lescinsky D. T., and Nesbitt H. W. (2004) The composition and evolution of primordial solutions on Mars, with application to other planetary bodies. Geochimica Cosmochimica Acta, 68, 4993-5008.

Klingelhöfer G., Morris R.V., Bernhardt B., Schröder C., Rodionov D. S., de Souza Jr. P. A., Yen A., Gellert R., Evlanov E. N., Zubkov B., and Foh J. (2004) Jarosite and hematite at Meridiani Planum from the Mössbauer spectrometer on the Opportunity rover. Science, 306, 1740-1745.

Koeberl C. (1993) Instrumental neutron activation analysis of geochemical and cosmochemical samples: a fast and reliable method for small sample analysis. Journal of Radioanalytical and Nuclear Chemistry, 168, 47-60.

Krissek L. A. and Kyle P. R. (2000) Geochemical indicators of weathering, Cenozoic paleoclimates, and provenance from fine-grained sediments in CRP-2/2A, Victoria Land Basin, Antarctica. Terra Antarctica, 7, 589-597.

Lane M. D. and Bishop J. L. (2019) Chapter 3: Mid-infrared (thermal) emission and reflectance spectroscopy, in: Bishop, J. L., Bell III, J. F., Moersch, J. E. (eds.), Remote Compositional Analysis: Techniques for Understanding Spectroscopy, Mineralogy, and Geochemistry of Planetary Surfaces. Cambridge: Cambridge University Press, 42-67.

Lane, M.D., Bishop J.L., Dyar M.D., King P.L., Parente M., and Hyde B.C. (2008) Mineralogy of the Paso Robles Soils on Mars. American Mineralogist, 93, 728-739.

Langevin H., Poulet F., Bibring, J. P. and Gondet B. (2005) Sulfates in the north polar region of Mars detected by OMEGA/Mars Express. Science, 307, 1584-1586.

Lee Y. I., Lim H. S., and Yoon, H. I. (2004) Geochemistry of soils of King George Island, South Shetland Islands, West Antarctica: Implications for pedogenesis in cold polar regions. Geochimica et Cosmochimica Acta, 68(21), 4319-4333.

Levy J. S., Fountain A. G., Gooseff M. N., Welch K. A., and Lyons H. B. (2011) Water tracks and permafrost in Taylor Valley, Antarctica: Extensive and shallow groundwater connectivity in a cold desert ecosystem. Geological Society of America Bulletin, 123, 2295-2311.

Li C. and Yang S. (2010) Is a chemical index of alteration (CIA) a reliable proxy for chemical weathering in global drainage basins? American Journal of Science, 310, 111-127.

Liu J., Michalski J. R., Zhou M-F. (2021) Intense subaerial weathering of eolian sediments in Gale crater, Mars. Science Advances, 7(32), eabh2687, 1-10.

Lyons H. B., Welch K. A., Fountain A. G., Dana G. L., Vaughn B. H., and McKnight D. M. (2003) Surface glaciochemistry of Taylor Valley, southern Victoria Land, Antarctica and its relationship to stream chemistry. Hydrological Processes, 17, 115-130.

Mader D. and Koeberl C. (2009) Using instrumental neutron activation analysis for geochemical analyses of terrestrial impact structures: current analytical procedures at the University of Vienna gamma spectrometry laboratory. Applied Radiation and Isotopes, 67, 2100-2103.

Mangold, N., Dehouck, E., Fedo, C., Forni, O., Achilles, C., Bristow, T., Downs, R. T., Frydenvang, J., Gasnault, O., L'Haridon, J., Le Deit, L., Maurice, S., McLennan, S. M., Meslin, P. Y., Morrison, S., Newsom, H. E., Rampe, E., Rapin, W., Rivera-Hernandez, F., Salvatore M., and Wiens, R. C. (2019). Chemical alteration of fine-grained sedimentary rocks at Gale crater. Icarus, 321, 619-631.

Marion G. M., Catling D. C., and Kargel J. S. (2009) Br/Cl partitioning in chloride minerals in the Burns formation on Mars. Icarus, 200, 436-445.

Marion G. M., Catling D. C., Kargel J. S., and Crowley J. K. (2016) Modeling calcium sulfate chemistries with applications to Mars. Icarus, 278, 31-37.

Masuda A., Nakamura N., Tanaka T. (1973) Fine structures of mutually normalized rare-earth patterns of chondrites. Geochimica Cosmochimica Acta, 43, 1131-1140.

McDonough W. F. and Sun S.-s. (1995) The composition of the Earth. Chemical Geology, 120, 223-253.

McGinnis L. D. and Jensen T. E. (1971) Permafrost-hydrogeologic regimen in two ice-free valleys, Antarctica, from electrical depth sounding. Quaternary Research, 1, 389-409.

McGinnis L. D., Nakao K., Clark C. C. (1973) Geophysical identification of frozen and unfrozen ground, Antarctica. 2nd International Conference on Permafrost. Washington, D.C., National Academy of Sciences, 136-146.

McLennan S. M., Bell J. F., Calvin W. M., Christensen P. R., Clark B. C., De Souza P., Farmer J., Farrand W., Fike D., Gellert R., Ghosh A., Glotch T., Grotzinger J. P., Hahn B., Herkenhoff K., Hurowitz J. A., Johnson J. R., Johnson S. S., Jolliff B., and Yen, A. (2005) Provenance and diagenesis of the evaporite-bearing Burns Formation, Meridiani Planum, Mars. Earth and Planetary Science Letters, 240, 95-121.

McLennan S. M., Anderson R. B., Bell III J. F., Bridges J. C., Calef III F., Campbell J. L., Clark B. C., Clegg S., Conrad P., Cousin A., Des Marais D. J., Dromart G., Dyar M. D., Edgar L.A., Ehlmann B. A., Fabre C., Forni O., Gasnault O., Gellert R., Gordon S., Grant J.A., Grotzinger J. P., Gupta S., Herkenhoff K. E., Hurowitz J.A., King P. L., Le Mouélic S., Leshin L.A., Léveillé R., Lew K.W., Mangold N., Maurice S., Ming D. W., Morris R. V., Nachon M., Newsom H. E., Ollila A. M., Perrett G. M., Rice M. S., Schmidt M. E., Schwenzer S. P., Stack K., Stolper E. M., Sumner D. Y., Treiman A. H., VanBommel S., Vaniman D. T., Vasavada A., Wiens R. C., Yingst R. A., and the MSL Science Team (2014) Elemental Geochemistry of Sedimentary Rocks at Yellowknife Bay, Gale Crater, Mars. Science, 343 (6169), Art. no. 1244734.1-1244734.32.

McLennan S. M., Dehouck E., Grotzinger J. P., Hurowitz J. A., Mangold N., Siebach K., and the MSL Science Team (2015) Geochemical record of open-system chemical weathering at Gale Crater

and Implications for paleoclimates on Mars. 46th Lunar and Planetary Science Conference, Abstract no. 1832.

McLeod M., Bockheim J., Balks M., Aislabie J. (2009) Soils of western Wright Valley, Antarctica. Antarctic Science, 21, 355-365.

McNamara J. P., Kane D. L., and Hinzman L. D. (1999) An analysis of an arctic channel network using a digital elevation model. Geomorphology, 29, 339-353.

McSween, Jr., H. Y. (2002) The rocks of Mars, from far and near. Meteoritics & Planetary Science 37, 7-25.

McSween Jr. H. Y. (2015) Petrology on Mars. American Mineralogist, 100, 2380-2395.

Meteoblue 2020 Weather Archive, Weather conditions at King Sejong Station, Antarctica, https://www.meteoblue.com/en/weather/historyclimate/weatherarchive/king-sejong-station_antarctica_6620761 (accessed July 2021).

Mernagh T. P., Miezitis Y., and Geoscience Australia. (2008). A review of the geochemical processes controlling the distribution of thorium in the Earth's crust and Australia's thorium resources. Canberra: Geoscience Australia, 1-49.

Meyer G. H., Morrow M. B., Wyss O., Berg T. E., and Littlepage J. L. (1962) Antarctica: the Microbiology of an unfrozen saline pond. Science, 138, 1103-1104.

Ming D. W., Archer P. D. Jr., Glavin D. P., Eigenbrode J. L., Franz H. B., Sutter B., Brunner A. E., Stern J. C., Freissinet C., McAdam A. C., Mahaffy P. R., Cabane M., Coll P., Campbell J. L., Atreya S. K., Niles P. B., Bell J. F. 3rd, Bish D. L., Brinckerhoff W. B., Buch A., Conrad P. G., Des Marais D. J., Ehlmann B. L., Fairén A. G., Farley K., Flesch G. J., Francois P., Gellert R., Grant J. A., Grotzinger J. P., Gupta S., Herkenhoff K. E., Hurowitz J. A., Leshin L. A., Lewis K. W., McLennan S. M., Miller K. E., Moersch J., Morris R. V., Navarro-González R., Pavlov A.

A., Perrett G. M., Pradler I., Squyres S. W., Summons R. E., Steele A., Stolper E. M., Sumner D. Y., Szopa C., Teinturier S., Trainer M. G., Treiman A. H., Vaniman D. T., Vasavada A. R., Webster C. R., Wray J. J., Yingst R. A., and the MSL Science Team. (2014) Volatile and organic compositions of sedimentary rocks in Yellowknife Bay, Gale crater, Mars. Science. 343 (6169), 1245267–1245267.

Morgan G. A., Head J. H., Marchant D. R., Dickson J. L., and Levy J. S. (2008) Interaction between gullies and lobate debris tongues on Mars and in the Antarctic Dry Valleys. 39th Lunar Planetary Science Conference, Abstract no. 2303.

Morris E. C., Mutch T. A., and Holt H. E. (1972) Atlas of geologic features in the dry valleys of South Victoria Land, Antarctica: possible analogs of martian surface features. U. S. Geological Survey USGS interagency report: Astrogeology, 52, 73-196, Reston, VA.

Morris, R. V., Vaniman, D. T., Blake, D. F., Gellert, R., Chipera, S. J., Rampe, E. B. Ming, D. W., Morrison, S. M., Downs, R. T., Treiman, A. H., Yen A. S., Grotzinger J. P., Achilles C. N., Bristow T. F., Crisp J. A., Des Marais D. J., Farmer J. D., Fendrich K. V., Frydenvang J., Graff T. G., Morookian J. M., Stolper E. M., and Schwenzer S. P. (2016) Silicic volcanism on Mars evidenced by tridymite in high-SiO2 sedimentary rock at Gale crater. Proceedings of the National Academy of Sciences, 113(26), 7071-7076.

Morrison A.D. (1989) Ferrar Dolerite Intrusions at Terra Cotta Mountain, Southern Victoria Land, Antarctica. M.Sc. Thesis, Dunedin, University of Otago, 165.

Morrison A. D and Reay A. (1995) Geochemistry of Ferrar Dolerite sills and dykes at Terra Cotta Mountain, south Victoria Land, Antarctica. Antarctic Science, 7(1), 73-85.

Murchie S. L ., Mustard J. F., Ehlmann B. L., Milliken R. E., Bishop J. L., McKeown N. K., Noe Dobrea E. Z., Seelos F. P., Buczkowski D. L., Wiseman S. M., Arvidson R. E., Wray J. J., Swayze G., Clark R. N., Des Marais D. J., McEwen A. S., Bibring J-P. (2009) A synthesis of

Martian aqueous mineralogy after 1 Mars year of observations from the Mars Reconnaissance Orbiter. Journal of Geophysical Research, 114, E00D06, 1-30.

Murray A. E., Kenig F., Fritsen C., McKay C., Cawley K., Edwards R., Kuhn E., Mcknight D., Ostrom N., Peng V., Ponce A., Priscu J., Samarkin V., Townsend A., Wagh P., Young S., Yung P., and Doran P. (2012) Microbial life at -13°C in the brine of an ice-sealed Antarctic lake. Proceedings of the National Academy of Sciences of the United States of America, 109(50), 20626-20631.

Nachon M., Clegg S. M., Mangold N., Schröder S., Kah L. C., Dromart G., Ollila A., Johnson J.R., Oehler D. Z., Bridges J. C., Le Mouélic S., Forni O., Wiens R. C., Anderson R.B., Blaney D. L., Bell III J. F., Clark B., Cousin A., Dyar M. D., Ehlmann B., Fabre C., Gasnault O., Grotzinger J., Lasue J., Lewin E., Léveillé R., McLennan S., Maurice S., Meslin P. -Y., Rapin W., Rice M., Squyres S. W., Stack K., Sumner D. Y., Vaniman D., and Wellington D. (2014) Calcium sulfate veins characterized by ChemCam/Curiosity at Gale crater, Mars. Journal of Geophysical Research: Planets, 119, 1991-2016.

ChemMin Data, NASA Planetary Data System, https://pds-geosciences.wustl.edu/msl/msl-m-chemin-4-rdr-v1/ (Accessed June 2022).

Nesbitt H. H. and Markovics G. (1997) Weathering of granodioritic crust, long term storage of elements in weathering profiles, and petrogenesis of siliciclastic sediments. Geochimica Cosmochimica Acta, 61, 1653-1670.

Nesbitt, H. H. and Young, G. M. (1982) Early Proterozoic climates and plate motions inferred from major element chemistry of lutites. Nature, 299, 715-717.

Nichols, G. (2009). Sedimentology and stratigraphy (2nd ed.), Ch. 6. Wiley-Blackwell, West Sussex, United Kingdom, 1-411.

Nyakairu G. H. A. and Koeberl C. (2001) Mineralogical and chemical composition and distribution of rare earth elements in clay-rich sediments from central Uganda. Geochemical Journal, 35, 13-28.

Oberts G. L. (1973) The chemistry and hydrogeology of dry valley lakes, Antarctica. Master's thesis, Northern Illinois University, DeKalb, 1-55.

Obryk M. K., Doran P. T., Fountain A. G., Myers M., and McKay C. P. (2020) Climate from the McMurdo Dry Valleys, Antarctica, 1986–2017: Surface air temperature trends and redefined summer season. Journal of Geophysical Research: Atmospheres, 125, 1-14.

Palmer K. (1990) XRF analyses of granitoids and associated rocks, St. Johns Range, south Victoria Land, Antarctica, Victoria University of Wellington Research School of Earth Sciences Geology Board of Studies, 5, 1-23.

Patel S. N., Bishop J. L., Englert P. A. J., and Gibson E. K. (2015) Coordinating Chemical and Mineralogical Analyses of Antarctica Dry Valley Sediments as Potential Analogs for Mars. 46th Lunar Planetary and Planetary Science Conference, Abstract no. 1537.

Parker, A. (1970) An index of weathering for silicate rocks. Geological Magazine, 107, 501-504.

Pérez E., and Chebude H. (2017) Chemical Analysis of Gaet'ale, a Hypersaline Pond in Danakil Depression (Ethiopia): New Record for the Most Saline Water Body on Earth. Aquatic Geochemistry, 23, 109-117.

Ragotzkie R. A. (1964) The Heat Balance of Two Antarctic Lakes. Limnology and Oceanography, 9, 412-425.

Rampe E. B., Ming D. W., Blake D. F., Bristow T. F., Chipera S. J., Grotzinger J. P., Morris R. V., Morrison S. M., Vaniman D. T., Yen A. S., Achilles C. N., Craig P. I., Des Marais D. J., Downs R. T., Farmer J. D., Fendrich K. V., Gellert R., Hazen R. M., Kah L. C., Morookian J. M., Peretyazhko T. S., Sarrazin P., Treiman A. H., Berger J. A., Eigenbrode J., Fairén A. G., Forni O., Gupta S., Hurowitz J. A., Lanza N. L., Schmidt M. E., Siebach K., Sutter B., and Thompson L. M. (2017) Mineralogy of an ancient lacustrine mudstone succession from the Murray formation, Gale crater, Mars. Earth and Planetary Science Letters, 471, 172-185.

Rice M. S., Bell III J. F., Godber A., Wellington D., Fraeman A. A., Johnson J. R., Kinch K. M., Malin M. C., and Grotzinger J. P. (2013), Mastcam Multispectral Imaging Results From the Mars Science Laboratory Investigation in Yellowknife Bay. European Planetary Science Congress, 8, Abstract No. 762.

Rice M. S., Gupta S., Treiman A. H., Stack K. M., Calef F., Edgar L. A., Grotzinger J. P., Lanza N., Le Deit L., Lasue J., Siebach K. L., Vasavada A., Wiens R. C., and Williams J. (2017) Geologic overview of the Mars Science Laboratory rover mission at the Kimberley, Gale crater, Mars. Journal Geophysical Research: Planets, 122, 2-20.

Robertson, K. and Bish D. (2013) Constraints on the distribution of $CaSO_4 \cdot nH_2O$ phases on Mars and implications for their contribution to the hydrological cycle. Icarus, 223, 407-417.

Sarrazin, P., Blake, D. F., Feldman, S., Chipera, S. J., Vaniman, D. T., and Bish, D. L. (2005) Field deployment of a portable X-ray diffraction/X-ray fluorescence instrument on Mars analog terrain. Powder Diffraction, 20, 128-133.

Sheldon N. D. and Tabor N. J. (2009) Quantitative paleoenvironmental and paleoclimatic reconstruction using paleosols. Earth-Science Reviews, 95, 1-52.

Siebach, K. L., Baker, M. B., Grotzinger, J. P., McLennan, S. M., Gellert, R., Thompson, L. M., and Hurowitz, J. A. (2017), Sorting out compositional trends in sedimentary rocks of the Bradbury group (Aeolis Palus), Gale crater, Mars. Journal of Geophysical Research: Planets, 122, 295-328

Siebach K. L., McLennan S. M. (2018) Re-Evaluating the CIA paleoclimate proxy on Mars at Curiosity's drill sites. 49thLunar and Planetary Science Conference, Abstract no. 2694.

Siebach K. L, Achilles C. N., Smith R. J., McLennan S. M., Dehouck E. (2020) Using Curiosity Drill Sites to Test the Chemical Index of Alteration, 51st Lunar and Planetary Science Conference, Abstract no. 3028.

Small H., Stevens T. S., Bauman H. C. (1975) Novel ion exchange chromatographic method using conductimetric detection. Analytical Chemistry, 47, 1801-1809.

Stack K. M., Grotzinger J. P., Lamb M. P., Gupta S., Rubin D. M., Kah L. C., Edgar L., Fey D., Hurowitz J. A., McBride M., Rivera-Hernandez F., Sumner D., Beek J. V., Williams R. M., and Yingst R. (2019). Evidence for plunging river plume deposits in the Pahrump Hills member of the Murray formation, Gale crater, Mars. Sedimentology, 66, 1768-1802.

Squyres, S.W., Grotzinger J.P., Arvidson R.E., Bell J.F., Calvin W., Christensen P.R., Clark B.C., Crisp J.A., Farrand W.H., Herkenhoff K.E., Johnson J.R., Klingelhöfer G., Knoll A.H., McLennan S.M., McSween H.Y., Morris R.V., Rice J.W., Rieder R., and Soderblom L.A. (2004) In Situ Evidence for an Ancient Aqueous Environment at Meridiani Planum, Mars. Science, 306, 1709.

Squyres S. W., Arvidson, R. E., Bell III J. F., Calef III F., Clark B. C., Cohen B.A., Crumpler L. A., de Souza Jr. P. A., Farrand, W. H., Gellert R., Grant J., Herkenhoff, K. E., Hurowitz, J. A., Johnson J. R., Jolliff B. L., Knoll A. H., Li R., McLennan S. M., Ming D. W., Mittlefehldt W., Parker T. J., Paulsen G., Rice M. S., Ruff S. W., Schröder C., Yen A. S., and Zacny K. (2012) Ancient Impact and Aqueous Processes at Endeavour Crater, Mars. Science, 336, 570-576.

Sueoka T. (1988) Identification and classification of granite residual soils using chemical weathering index. Second International Conference Geomechanics in Tropical Soils, Singapore, 55-61.

Szynkiewicz A. and Bishop J. L. (2021) Assessment of Sulfate Sources under Cold Conditions as a Geochemical Proxy for the Origin of Sulfates in the Circumpolar Dunes on Mars. Minerals, 11(5), 507, 2-20.

Taylor G. J., Stopar J. D., Boynton W. V., Karunatillake S., Keller J. M., Brückner J., Wänke H., Dreibus G., Kerry K. E., Reedy R. C., Evans L. G., Starr R. D., Martel L. M. V., Squyres S. W., Gasnault O., Maurice C. d'Uston S., Englert P., Dohm J. M., Baker V. R., Hamara D., Janes D., Sprague A. L., Kim K. J., Drake D. M., McLennan S. M., and Hahn B. C. (2006) Variations in K/Th on Mars. Journal of Geophysical Research, 111, 2-20.

Taylor S. R. and McLennan S. M. (1985) The Continental Crust: Its Composition and Evolution. Blackwell Scientific Publication, Oxford, United Kingdom, 1-312.

Thompson D. C., Bromley A. M., Craig R.M.F. (1971b) Ground temperatures in an Antarctic dry valley. New Zealand Journal of Geology and Geophysics, 14, 477-483.

Thompson L. M., Schmidt M., Perrett G., Elliott B., Gellert R., Fisk M., and the APXS team. (2014) K-rich rocks at Gale, Dingo gap to the Kimberley: An APXS perspective. 8th International Conference on Mars, Pasadena, California, Abstract No. 1791, 1433.

Thompson L. M., Schmidt, M. E. Spray J. G., Berger J. A., Fairén A. G., Campbell J. L., Perrett G. M., Boyd N., Gellert R., Pradler I., VanBommel S. J. (2016a) Potassium-rich sandstones within the Gale impact crater, Mars: The APXS perspective. Journal of Geophysical Research: Planets, 121, 1981-2003.

Thompson L. M., Schmidt M. E., Gellert R., Spray J.G., and the MSL APXS Team (2016b) APXS compositional trends along Curiosity's traverse, Gale Crater, Mars: Implications for crustal composition, sedimentary provenance, diagenesis and alteration. 47th Lunar Planetary Science Conference, Abstract no. 2709.

Thorpe M. T., Hurowitz J. A., and Siebach K. L. (2021) Weathering and Sedimentation in Basaltic Terrains on Earth; Implications for the Paleoclimate of Gale Crater, Mars. Workshop on Terrestrial Analogs for Planetary Exploration, Lunar Planetary Institute, Contribution, Abstract No. 8064.

Toner J. D. (2012) Using Salt Accumulations and Luminescence Dating to Study the Glacial History of Taylor Valley, Antarctica. Doctoral thesis. University of Washington, Seattle, 1-261.

Toner J. D., Sletten R. S., Liu L., Catling D.C., Ming D. W., Mushkin A., and Lin P-C. (2022) Wet Streak in the McMurdo Dry Valleys, Antarctica: Implications for Recurring Slope Lineae on Mars. Earth and Planetary Science Letter, 589, 117582.

Torii T. and Osaka J. (1965) Antarcticite: A New Mineral, Calcium Chloride Hexahydrate, Discovered in Antarctica. Science, 149, 975-977.

Torii T., Murata S., Yamagata N. (1981) Geochemistry of the Dry Valley Lakes. Journal of the Royal Society of New Zealand 11, 387-399.

Tosca N. J. and McLennan S. M., (2006) Chemical divides and evaporite assemblages on Mars. Earth and Planetary Science Letters, 241, 21-31.

Tosca N. J., McLennan S. M., Lindsley D.H., Schoonen M. A. A. (2004) Acid–sulfate weathering of synthetic Martian basalt: the acid fog model revisited. Journal of Geophysical Research: Planets, 109, 1-29.

Treiman A. H., Bish, D. L., Vaniman, D. T., Chipera, S. J., Blake, D. F., Ming, D. W., Morris, R. V., Bristow, T. F., Morrison, S. M., Baker, M. B., Rampe E. B., Downs R. T., Filiberto J., Glazner A. F., Gellert R, Thompson L. M., Schmidt M. E., Le Deit L., Wiens R. C., McAdam A. C., Achilles C. N., Edgett K. S., Farmer J. D., Fendrich K. V., Grotzinger J. P., Gupta S., Morookian J. M., Newcombe M. E., Rice M. S., Spray J. G., Stolper E. M., Sumner D. Y., Vasavada A. R., Yen A. S. (2016) Mineralogy, provenance, and diagenesis of a potassic basaltic sandstone on Mars: CheMin X-ray diffraction of the Windjana sample (Kimberley area, Gale crater). Journal of Geophysical Research: Planets, 121, 75-106.

Tu V. M., Rampe E. B., Bristow T. F., Thorpe M. T., Clark J. V., Castle N., Fraeman A. A., Edgar L. A., McAdam A., Bedford C., Achilles C. N., Blake D., Chipera S. J., Craig P. I., Des Marais D. J., Downs G. W., Downs R. T., Fox V., Grotzinger J. P., Hazen R. M., Ming D. W., Morris R. V., Morrison S. M., Pavri B., Eigenbrode J., Peretyazhko T. S., Sarrazin P. C., Sutter B., Treiman A. H., Vaniman D. T., Vasavada A. R., Yen A. S., Bridges J. C. (2021) A Review of the Phyllosilicates in Gale Crater as Detected by the CheMin Instrument on the Mars Science Laboratory, Curiosity Rover. Minerals. 11(8): 847, 1-36.

Vaniman, D., Bristow T. F., Blake D., Des Marais D., Achilles C., Spanovich N., Vasavada A., Robert Anderson, Crisp J., Morookian J. M., Yen A., Bish D., Chipera S., Robert D., Shaunna M., Farmer J., Grotzinger J., Stolper E., Morris R., Ming D., Rampe E., Treiman A., Sarrazin P. and the MSL Science Team. (2013) Data from the Mars Science Laboratory CheMin XRD/XRF instrument. Geophysical Research Abstracts, 15, Abstract no. 6272.

Vaniman D. T., Bish D. L., Ming D. W., Bristow T. F., Morris R. V., Blake D. F., Chipera S. J., Morrison S. M., Treiman A. H., Rampe E. B., Rice M., Achilles C. N., Grotzinger J. P., McLennan S. M., Williams J., Bell III J. F., Newsom H. E., Downs R. T., Maurice S., Sarrazin P., Yen A. S., Morookian J. M., Farmer J. D., Stack K., Milliken R. E., Ehlmann B. L., Sumner D. Y., Berger G., Crisp J. A., Hurowitz J. A., Anderson R., Des Marais D. J., Stolper E. M., Edgett K. S., Gupta S., Spanovich N., and the MSL Science Team. (2014) Mineralogy of a mudstone at Yellowknife Bay, Gale Crater, Mars. Science, 343, 1243480, 1-23.

Vaniman D. T., Martínez,G. M., Rampe E. B., Bristow T. F., Blake D. F., Yen A. S., Ming D. W., Rapin W., Meslin P. Y., Morookian, J. M., Downs R. T., Chipera S. J., Morris R. V., Morrison S. M., Treiman A. H., Achilles C. N., Robertson K., Grotzinger J. P., Hazen R. M., Wiens R.C., and Sumner D. Y. (2018) Gypsum, bassanite, and anhydrite at Gale crater, Mars. American Mineralogist, 103, 1011-1020.

Van Driessche A. E. S., Stawski T. M., Benning L. G., and Kellermeier M. (2017) Calcium sulfate precipitation throughout its phase diagram. In New Perspectives on Mineral Nucleation and Growth, Ch. 12, 227-256.

Vasavada A. R. (2022) Mission Overview and Scientific Contributions from the Mars Science Laboratory Curiosity Rover After Eight Years of Surface Operations. Space Science Reviews, 218(3): 14, 1-65.

Velbel M. A. (2012) Aqueous alteration in Martian meteorites: Comparing mineral relations in igneous-rock weathering of Martian meteorites and in the sedimentary cycle of Mars. In Sedimentary

Geology of Mars (eds. J. P. Grotzinger and R. E. Milliken). SEPM Special Publication 102, 97-112.

Weitz C. M., Noe Dobrera E., and Wray J. J. (2015) Mixtures of clays and sulfates within deposits in western Melas Chasma, Mars. Icarus, 251, 291–314.

Wentworth S. J., Gibson E. K., Velbel M. A., and McKay D. S. (2005) Antarctic Dry Valleys and indigenous weathering in Mars meteorites: Implications for water and life on Mars. Icarus, 174, 383-395.

Wharton R. A., McKay C. P., Mancinelli R. L., and Simmons G. M., Jr. (1989) Early martian environments: the Antarctic lake. Advances in Space Research, 9, 147-153.

Yamagata N., Torii T., Murata S., and Watanuki K. (1967) Report of the Japanese summer parties in Dry Valleys, Victoria Land, 1963-65: 7. Chemical composition of pond waters in Ross Island with reference to those in Ongul Islands. Antarctic Record (Japan), 29, 2368-2375.

Yen, A. S., Morris R. V., Clark B. C., Gellert R., Knudson A. T., Squyres S. W., Mittlefehldt D. W., Ming D. W., Arvidson R., Mccoy T., Schmidt M., Hurowitz J., Li R., and Johnson J. R. (2008) Hydrothermal processes at Gusev Crater: An evaluation of Paso Robles class soils. Journal of Geophysical Research, 113, E06S10, doi:10.1029/2007JE002978.

Yen, A. S., Ming, D. W., Vaniman, D. T., Gellert, R., Blake, D. F., Morris, R. V., Morrison, S. M., Bristow, T. F., Chipera, S. J., Edgett, K. S., Treiman A. H, Clark B. C., Downs R. T., Farmer J. D., Grotzinger J. P., Rampe E. B., Schmidt M. E., and Sutter B. (2017) Multiple stages of aqueous alteration along fractures in mudstone and sandstone strata in Gale crater, Mars. Earth and Planetary Science Letters, 47, 186-198.

Yusa, H., (1972) The re-evaluation of heat balance in Lake Vanda, Victoria Land, (Jap.): in Contributions, Geophysical Institute, Kyoto University, 12, 87-100.

Figure 1. a) The continent of Antarctica and the McMurdo Dry Valleys, Source: Murray et al. 2012. b) The McMurdo Dry Valleys, Antarctica (~ 77.5° S, ~ 162.5° E)

Figure 2. a) Wright Valley, Antarctica (77°31′47″S 161°34′32″E: Lake Vanda, Central Wright Valley). Research areas are in the South Fork of Wright Valley. b) Location of sample cores from Don Juan Basin (77°33′52″S 161°10′20″E: Don Juan Pond, Central Don Juan Basin). Core 2074 is in Don Juan Pond; Cores 33 and 39 are 150 m and 300 m southwest of Core 2074, respectively. Core sampling depths are indicated to the left of the location markers.

Figure 3. Rare Earth Element (REE) abundances in Don Jan Basin samples normalized to C1-chondrites (Taylor and McLennan, 1985). Sample sets are color-coded by location. Sample depths can be inferred from Table 3. Average light REE abundances increase with distance from Core 2074.

Figure 4. a) Core 2074 soluble ion abundances for Na^{+}, Ca^{2+}, and Cl^{-}. b) Core 33 soluble ion abundances for Na^{+}, Ca^{2+}, and Cl^{-}. c) Core 39 soluble ion abundances for Na^{+}, Ca^{2+}, and Cl^{-}.

Figure 5. a) Reflectance spectra of Core 2074 from 0-5 μm. Absorption features diagnostic of gypsum are seen at about 1.9 and 2.5 μm. Features diagnostic of ferrihydrite are seen at about 1.4 μm. b) Reflectance spectra of Core 2074 from 2000-500 cm^{-1}. Strong absorption features diagnostic of anhydrite are seen at about 1200, 1450, and 1600 cm^{-1}. A weaker absorption features diagnostic of gypsum is seen at about 1800 cm^{-1}.

Figure 6. a) Reflectance spectra of Core 33 from 0-5 μm. A broad absorption band near 1 μm is due to pyroxene and a strong band at 4.68 μm for sample JB1132 (8-10 cm depth) indicates the presence of anhydrite. Bands near 1.2 and 2 μm are attributed to bassanite. Additional weak bands near 2.35 and 2.45 μm are due to OH bands in mica (e.g. biotite) or actinolites (e.g. tremolite). b) Reflectance spectra of Core 33 from 2000-500 cm^{-1}. Si-O stretching vibrations due to quartz are seen across most of the range, and absorption features at about 1600 cm^{-1} are likely due to anhydrite.

Figure 7. a) Reflectance spectra of scooped material sampled near Core 39 from 0.5-2.5 μm. b) Reflectance spectra of scooped material sampled near Core 39 from 0-5 μm. Spectral analysis of Core

39 (Figure 7) shows primarily quartz, feldspar, and pyroxene. Spectral bands characteristic of gypsum near 2 and 2.5 μm (Bishop, 2019) are strongest in the upper sediments (3-4 cm and 5-6 cm). Bands near 1.39, 1.93, and 2.19 μm are attributed to poorly crystallized aluminosilicates similar to allophane and are strongest in the lower sediments. The presence of allophane instead of crystalline clay minerals indicates limited soil maturity (Patel et al., 2015).

Figure 8. Comparison of Al_2O_3, TiO_2, and Fe_2O_3 abundances of DJP cores 2074, 33, and 39. Oxide abundances have been summed and each oxide's individual abundance is plotted as a percent of the sum. All core samples exhibit comparable abundances of Fe_2O_3, however, starting from the center of Don Juan Pond with Core 2074, both Al_2O_3 and TiO_2 abundances increase on average with distance from the pond, i.e from Core 2074 to Core 39. Local geologic constituents "Granitoids", "Beacon Sandstone", and "Ferrar Dolerite" oxide abundances are included for comparison. Local geologic constituent averages of "Granitoids" (Palmer, 1987, 1990; Ellery, 1989), "Beacon Sandstone", and "Ferrar Dolerite" (Grapes et al., 1989; Morrison and Reay, 1995) are included in Figure 8 to further constrain the degree of chemical alteration taking place at each core. Because the basin floor is likely predominantly Ferrar Dolerite (Peterson and Marsh, 2008), the observation that Core 2074 samples have oxide abundances close to those of Granitoids supports a dilution effect resulting from surrounding high salt content. This then would suggest active chemical alteration at Core 2074.

Figure 9. K/Th ratio of DJP core samples, normalized to an average terrestrial K/Th ratio of 2900 (Jagoutz et al., 1979; Taylor and McLennan 1985; McDonough and Sun, 1995; Taylor et al., 2006), is shown as a function of K abundance. K/Th ratios of the three local geologic constituents "Granitoids" (Palmer, 1987, 1990; Ellery, 1989), "Ferrar Dolerite" (Grapes et al., 1989; Morrison, 1995), and Barton Peninsula Rocks and Soils (Lee et al., 2004) are included for comparison.

Figure 10. Th/U vs depth. Core 2074, in the center of Don Juan Pond, has the lowest Th/U values while Th/U values increase towards Cores 33 and 39, 150 and 300 m to the southwest, respectively.

Figure 11. a) Uncorrected Chemical Index of Alteration (CIA) values for Don Juan Basin core samples plotted as a function of the molar ratio of Al_2O_3/TiO_2. CIA values display an unexpected chemical alteration gradient, with Core 2074 exhibiting the lowest degree of chemical alteration, Core 33

1593 enhanced chemical alteration, and Core 39 the highest degree of chemical alteration. b) The salt-
1594 corrected Chemical Index of Alteration values (CIA_{Salt}) for Don Juan Basin core samples plotted as a
1595 function of the molar ratio of Al_2O_3/TiO_2. All samples from all three cores' CIA values are now higher
1596 as a result of the salt correction and display the expected chemical alteration gradient. c) Uncorrected
1597 and corrected Chemical Index of Alteration (CIA and CIA_{Salt}) values for Don Juan Basin Core 2074
1598 samples and rock and soil samples taken by the rover Curiosity plotted as a function of the molar ratio of
1599 Al_2O_3/TiO_2.
1600

This is the peer-reviewed, final accepted version for American Mineralogist, published by the Mineralogical Society of America.
The published version is subject to change. Cite as Authors (Year) Title. American Mineralogist, in press.
DOI: https://doi.org/10.2138/am-2022-8779. http://www.minsocam.org/

1601 Figure 1

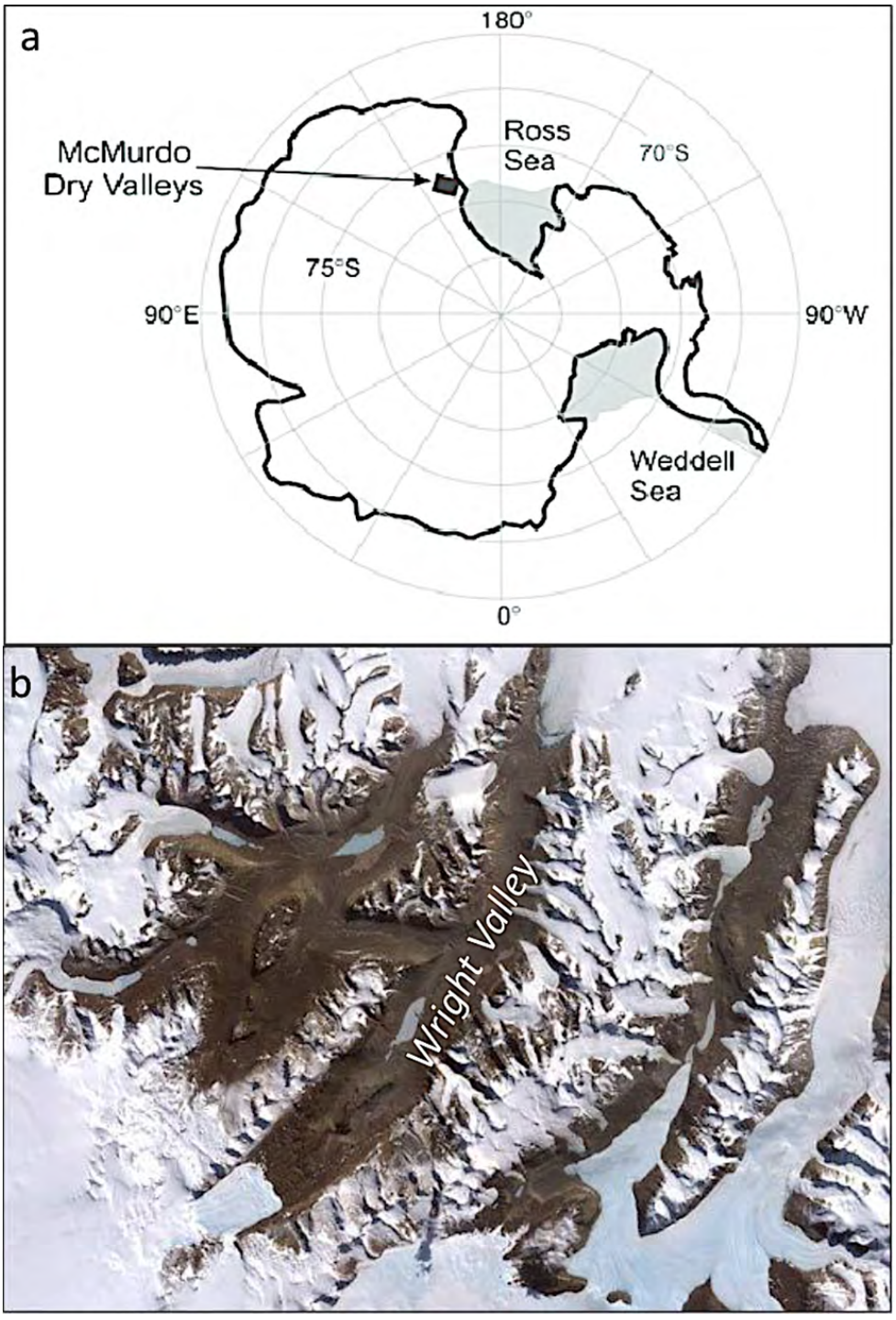

1602

1603 Figure 2

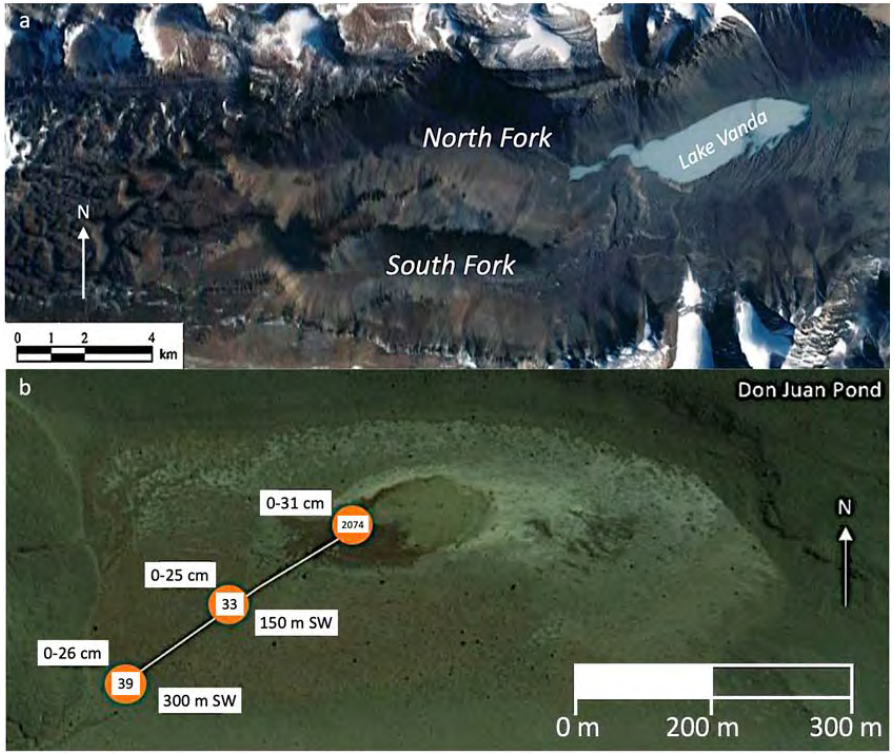

1604
1605
1606
1607
1608
1609
1610
1611
1612

1613 Figure 3

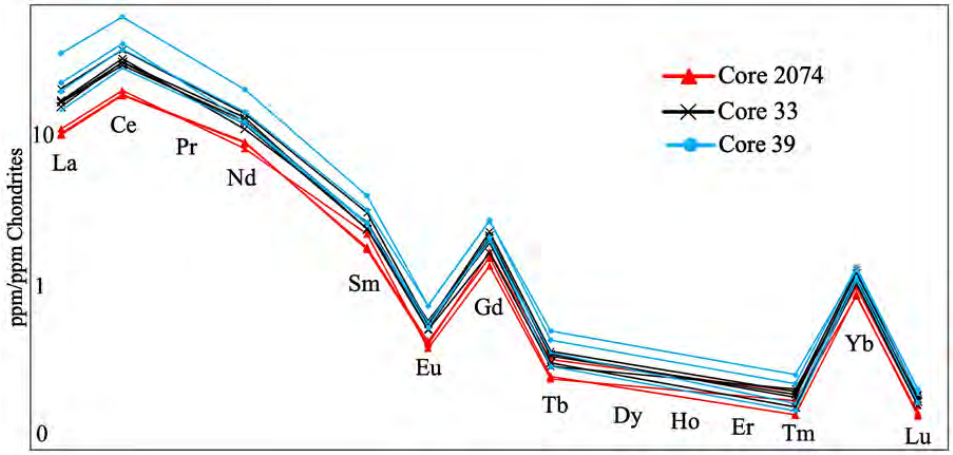

1614

1615

This is the peer-reviewed, final accepted version for American Mineralogist, published by the Mineralogical Society of America.
The published version is subject to change. Cite as Authors (Year) Title. American Mineralogist, in press.
DOI: https://doi.org/10.2138/am-2022-8779. http://www.minsocam.org/

1616 Figure 4

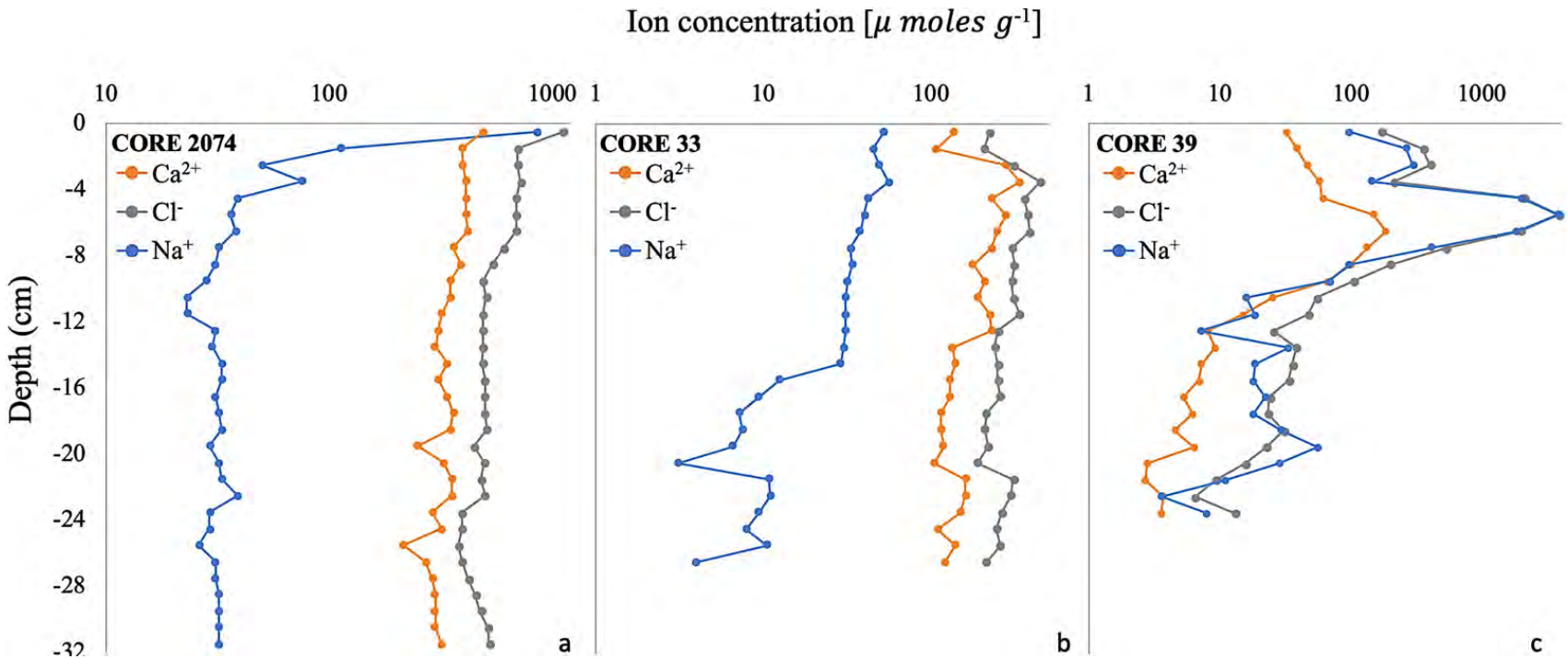

1617

This is the peer-reviewed, final accepted version for American Mineralogist, published by the Mineralogical Society of America.
The published version is subject to change. Cite as Authors (Year) Title. American Mineralogist, in press.
DOI: https://doi.org/10.2138/am-2022-8779. http://www.minsocam.org/

1618 Figure 5

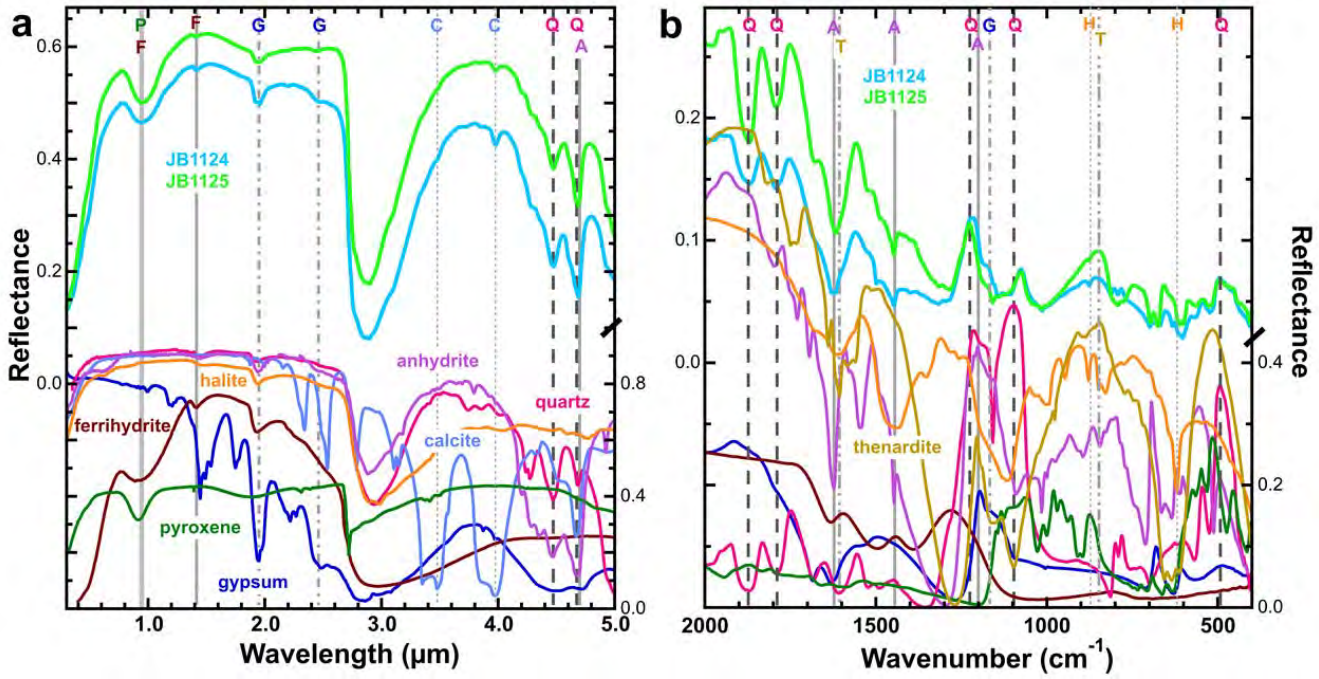

1619

1620

This is the peer-reviewed, final accepted version for American Mineralogist, published by the Mineralogical Society of America.
The published version is subject to change. Cite as Authors (Year) Title. American Mineralogist, in press.
DOI: https://doi.org/10.2138/am-2022-8779. http://www.minsocam.org/

1621 Figure 6

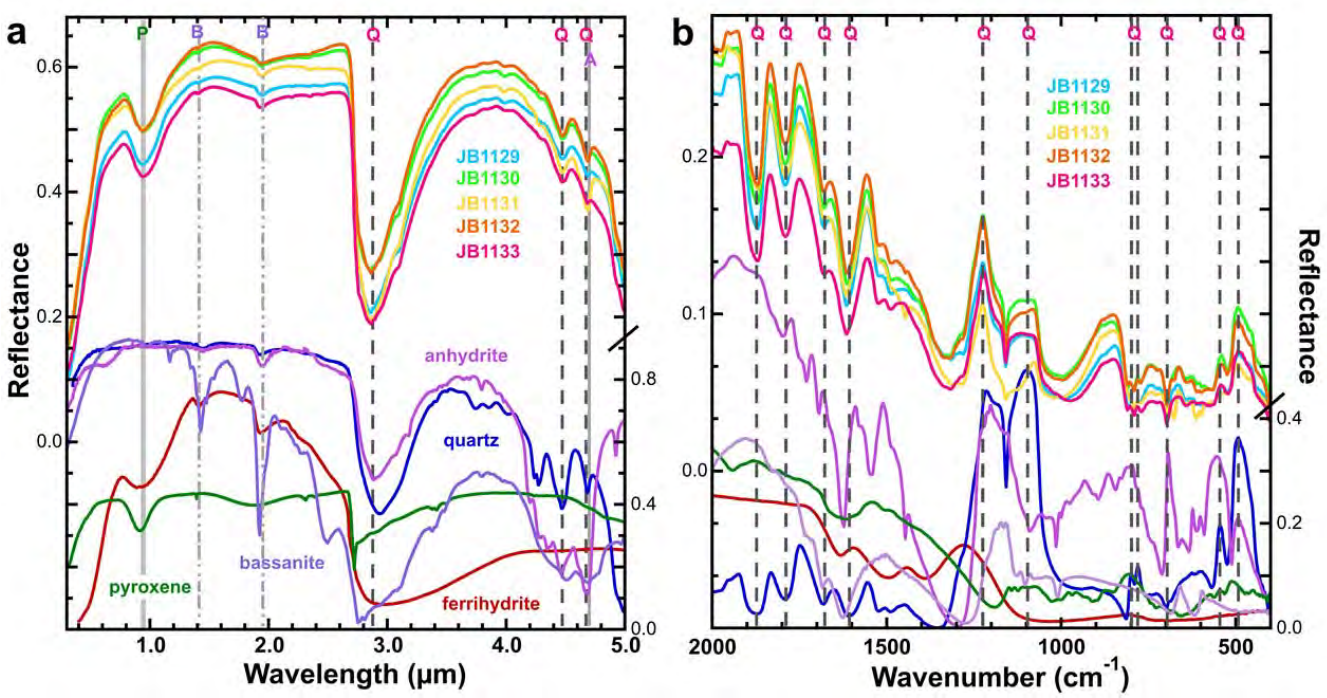

1622

1623

This is the peer-reviewed, final accepted version for American Mineralogist, published by the Mineralogical Society of America.
The published version is subject to change. Cite as Authors (Year) Title. American Mineralogist, in press.
DOI: https://doi.org/10.2138/am-2022-8779. http://www.minsocam.org/

1624 Figure 7

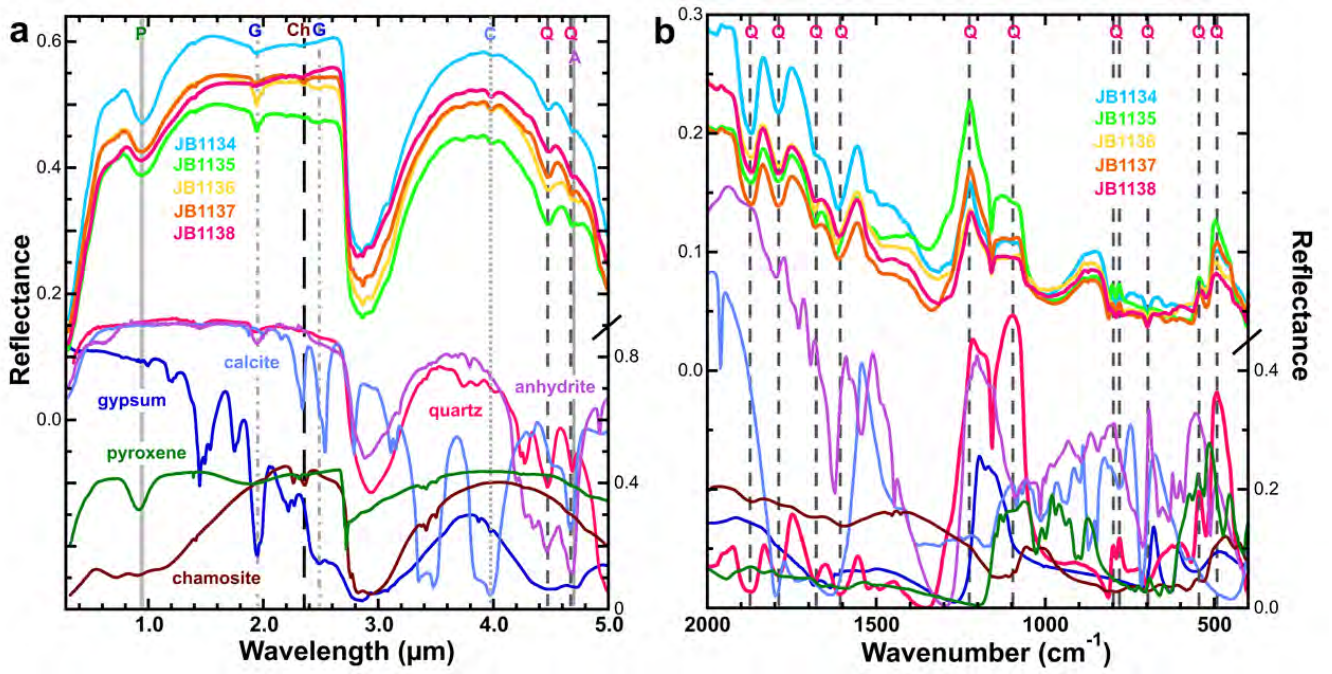

1625

1626

1627 Figure 8

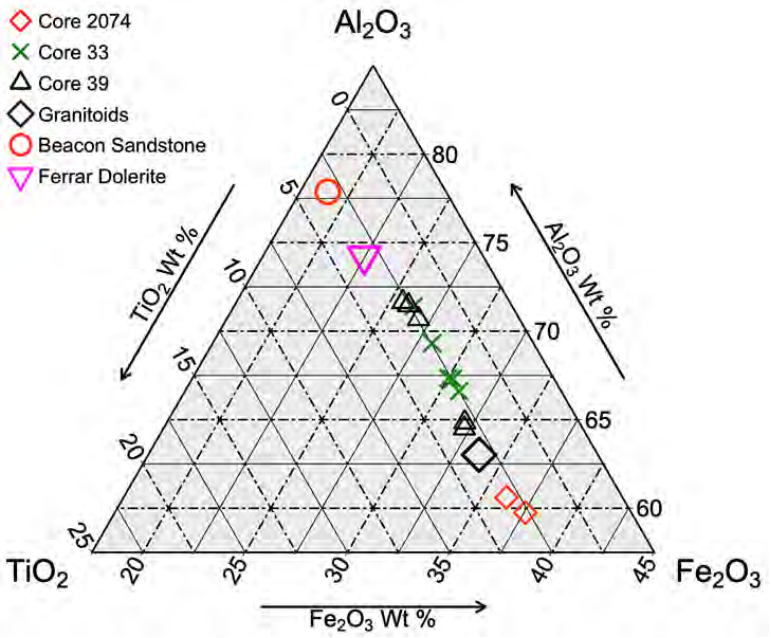

1628

1629

This is the peer-reviewed, final accepted version for American Mineralogist, published by the Mineralogical Society of America.
The published version is subject to change. Cite as Authors (Year) Title. American Mineralogist, in press.
DOI: https://doi.org/10.2138/am-2022-8779. http://www.minsocam.org/

1630 Figure 9

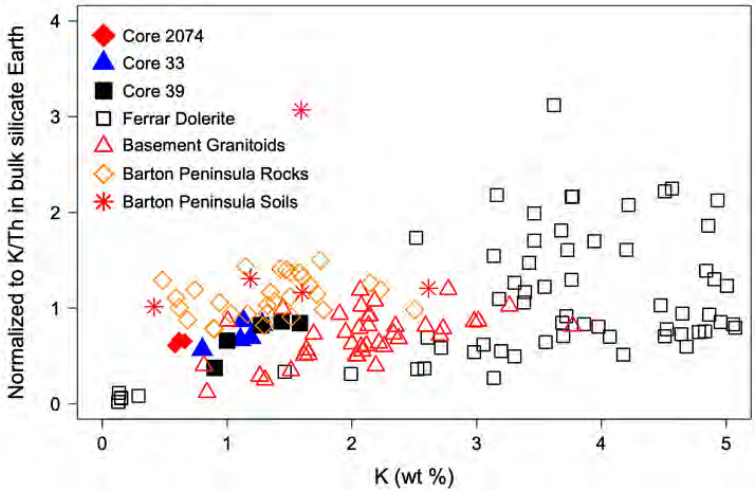

1631

1632

1633 Figure 10

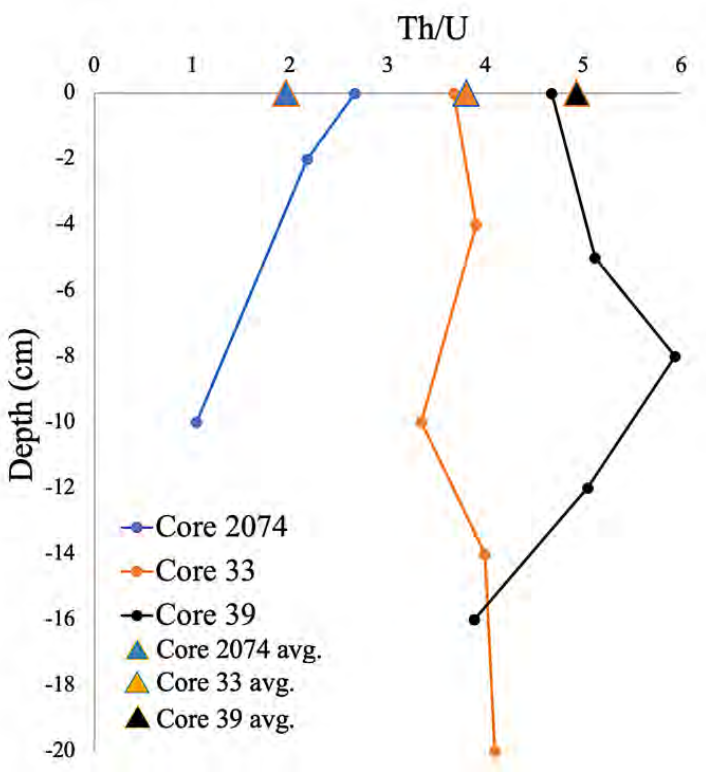

1634

1635

This is the peer-reviewed, final accepted version for American Mineralogist, published by the Mineralogical Society of America.
The published version is subject to change. Cite as Authors (Year) Title. American Mineralogist, in press.
DOI: https://doi.org/10.2138/am-2022-8779. http://www.minsocam.org/

1636 Figure 11

1637

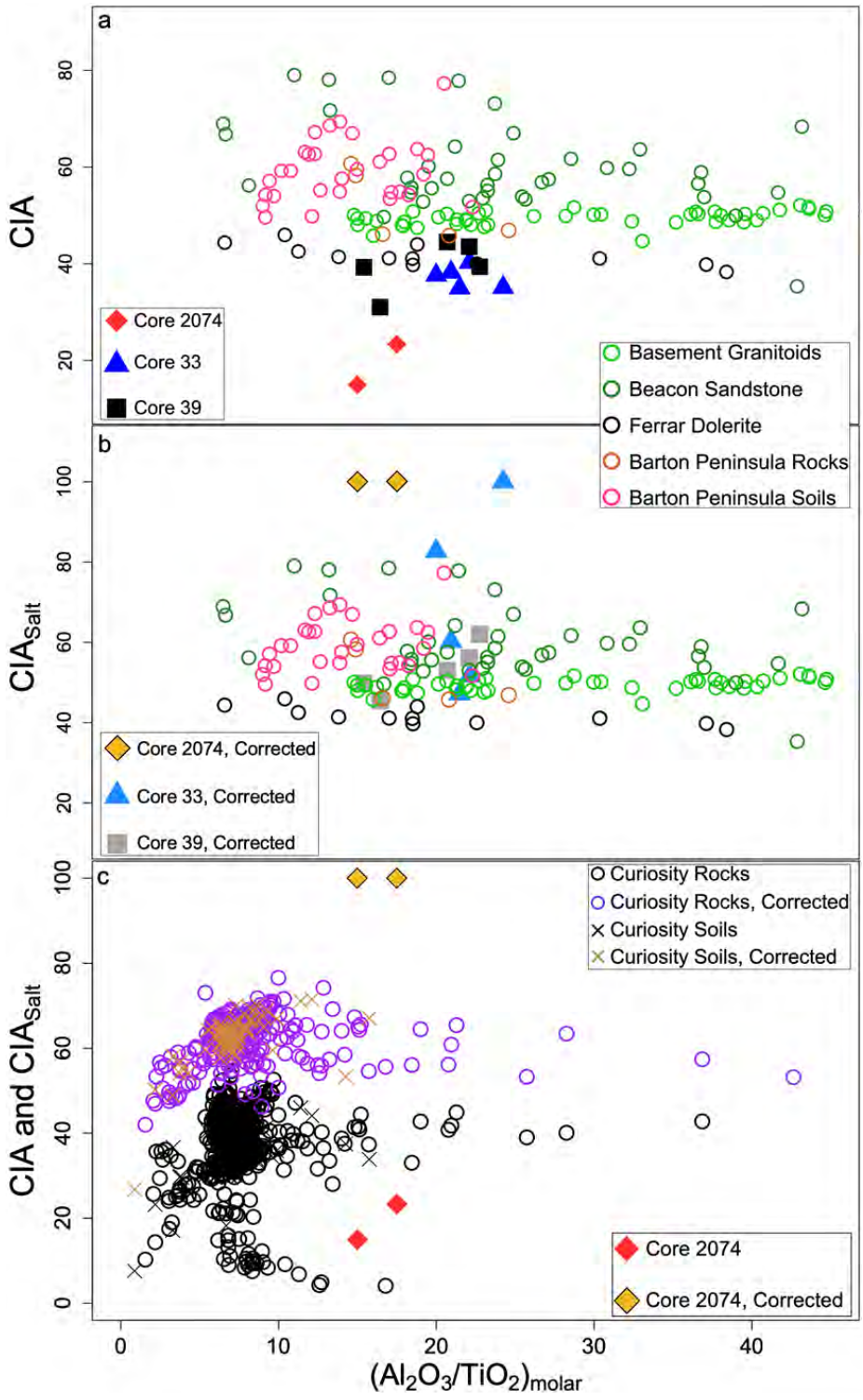

1638

Table 1. Don Juan Basin sample locations and information.

Core #	**Core ID**	Sample Depth (cm)	Additional Sample Information
Core 2074, center of Don Juan Pond, appx. 116 m above sea level	**JB1126**	0-1	White encrustations at surface
	JB1124	1-2	No encrustations
	JB1125	8- 10	Sediment to 10 cm depth
Core 33, 150 m SW of Core 2074, appx. 116.4 m above sea level	**JB1129**	0-1	
	JB1130	3-4	
	JB1131	8-10	Dark layer
	JB1132	12-14	Darkest layer
	JB1133	16-20	
Core 39, 300 m SW of Core 2074, appx. 117 m above sea level	**JB1134**	0-1	
	JB1135	2-5	
	JB1136	6-8	White layer
	JB1137	10-12	
	JB1138	15-16	Dark layer

Table 2. Elemental abundances of major and minor elements of sediments from Cores 2074, 33, and 39 in Don Juan Basin, Antarctica. Abundance is measured in weight percent (wt %).

Depth (cm)	**1-2**	**8-10**	**0-1**	**3-4**	**8-10**	**12-14**	**16-20**	**0-1**	**2-5**	**6-8**	**10-12**	**15-16**
Core ID	**JB1124**	**JB1125**	**JB1129**	**JB1130**	**JB1131**	**JB1132**	**JB1133**	**JB1134**	**JB1135**	**JB1136**	**JB1137**	**JB1138**
SiO_2	51.51	66.3	68.69	72.25	68.39	71.64	72.5	68.87	63.81	69.9	70.97	70.83
Al_2O_3	5.74	6.25	7.95	8.28	8.97	8.42	8.75	9.44	8.39	9.87	10.71	11.09
Fe_2O_3	3.43	3.93	3.97	4.27	3.67	4.17	3.96	5.24	4.61	4.17	4.33	4.41
MgO	2.52	3.23	3.57	3.84	3.3	3.75	3.56	4.71	4.15	3.75	3.9	3.97
CaO	16.67	9.81	3.25	3.51	2.78	3.29	3.19	4.23	3.68	3.33	3.27	3.25
Na_2O	0.95	1.05	5.03	4.64	6.3	5.23	4.56	5.03	4.65	4.39	4.1	4.2
K_2O	0.71	0.9	2.49	2.03	2.02	1.77	1.88	2.31	5.25	3.14	2.47	2.54
TiO_2	0.3	0.28	1.43	1.47	1.68	1.42	1.47	1.54	1.45	1.9	2.19	1.87
P_2O_5	0.05	0.04	0.29	0.31	0.29	0.33	0.31	0.48	0.4	0.34	0.38	0.42
MnO	0.06	0.07	0.05	0.06	0.06	0.07	0.06	0.12	0.08	0.07	0.09	0.1
Cr_2O_3	0.01	0.016	0.07	0.08	0.07	0.09	0.08	0.1	0.09	0.08	0.08	0.08
SO_4	14.43	8.88	0.24	0.48	3.74	1.34	0.08	n.d.	0.56	0.66	0.06	n.d.
SO_3	n.d.	n.d.	0.2	0.4	3.12	1.12	0.07	n.d.	0.47	0.55	0.05	n.d.
S	4.81	2.96	0.08	0.16	1.24	0.44	0.02	n.d.	0.18	0.22	0.02	n.d.
$CaSO_4$	20.85	11.67	n.d.	0.33	0.67	5.30	1.91	0.12	n.d.	0.80	0.93	0.08
Na_2SO_4	21.75	12.18	n.d.	0.35	0.70	5.53	1.99	0.13	n.d.	0.84	0.97	0.08
K_2SO_4	26.68	14.94	n.d.	0.43	0.86	6.79	2.44	0.16	n.d.	1.03	1.19	0.10
$MgSO_4$	18.43	10.32	n.d.	0.30	0.60	4.69	1.68	0.11	n.d.	0.71	0.82	0.07
$CaCl_2$	11.91	7.01	2.32	2.51	1.99	2.35	2.28	3.02	2.63	2.38	2.34	2.32
NaCl	0.7	0.77	3.73	3.44	4.67	3.88	3.38	3.73	3.44	3.25	3.04	3.11
CIA	14.95	23.33	34.96	38.24	35.08	37.62	40.27	39.24	31.01	39.63	43.53	44.48
CIA_{Salt}	100*	100*	47.19	60.24	100*	82.7*	51.61	49.85	45.51	62.0	56.15	53.02

Notes: Oxide data were determined by XRF; S abundance was measured via LECO combustion; sulfate and chloride abundances, including Na, K, Mg, and Ca, were calculated separately. Calculated CIA and CIA_{Salt} values are included for comparison. Asterisked CIA_{Salt} values indicate a likely overcorrection for measured salt. However, these values provide a better representation of the degree of chemical alteration than the uncorrected CIA.

Table 3. Elemental abundances of major, minor, and trace elements of sediments from Cores 2074, 33, and 39 in Don Juan Basin, Antarctica.

Core ID	**2074**	**2074**	**2074**	**33**	**33**	**33**	**33**	**33**	**39**	**39**	**39**	**39**	**39**
Depth (cm)	**0-1**	**1-2**	**8-10**	**0-1**	**3-4**	**8-10**	**12-14**	**16-20**	**0-1**	**2-5**	**6-8**	**10-12**	**15-16**
Elements (ppm)													
Na (wt %)	0.8	0.77	0.78	2.1	1.59	1.63	1.39	1.39	1.89	4.08	2.2	1.98	2.05
K (wt %)	0.66	0.61	0.58	1.28	1.11	1.19	1.13	0.8	1.27	1	1.6	0.9	1.44
Sc	14.9	13.6	17.1	16.5	16.8	13	15.7	14.4	20.1	17.9	15	16.8	14.7
Cr	127	82.1	114	121	119	92.9	109	99.7	146	126	100	116	104
Fe (wt %)	2.4	2.41	2.81	2.91	2.96	2.58	2.89	2.58	3.81	3.2	2.7	3.17	3.06
Co	14.5	13.3	16.9	16.8	17.4	13.3	16	14.7	21.1	18	14	16.6	15.5
Ni	33	37	46	53	52	44	37	36	57	52	34	53	42
Zn	40	37	41	51	50	46	50	46	62	54	47	58	58
Ga	5	2	5	21	9	7	8	17	9	21	12	17	42
As	<1.0	0.51	<0.8	<1.8	<1.3	<1.3	<1.2	0.26	<1.3	<2	<1.5	<1.8	0.59
Se	<1.6	<1.7	<1.8	<1.8	<1.7	<1.6	<1.2	<1.5	<2.3	<1.8	<1.5	<1.8	<2.7
Br	0.3	6.2	2.7	1.8	1.5	2.1	1.6	2.2	<1.1	<1.4	<1.1	<1.3	0.1
Rb	28.5	26.9	32.3	51.4	52.8	64	49	43.9	55.6	53.9	55	79.5	63.6
Sr	44	149	83	130	96	123	109	92	124	89	87	115	154
Zr	108	166	91	136	150	148	142	126	174	159	135	178	242
Sb	<0.2	<0.2	0.06	<0.2	<0.2	<0.2	<0.2	<0.2	<0.2	<0.3	<0.2	<0.2	0.08
Cs	0.77	0.98	1.01	1.23	1.16	1.7	1.9	1.83	1.37	1.13	1.1	1.47	1.69
Ba	123	127	131	220	245	235	205	195	262	219	211	301	365
La	11.4	12.4	11.7	18.5	19	22.7	17.3	18.6	21.9	16.4	25	38.8	26.1
Ce	20.6	22	20.9	32.3	35.6	40.7	33.9	33.8	41	30.8	45	66.7	44.8
Nd	10.1	9.21	10.2	14	12.4	15.5	14.6	13.3	16	13.4	14	22.4	14.5
Sm	2.09	2.56	2.02	3.02	3.05	3.52	2.75	2.78	3.68	2.96	3	4.56	3.7
Eu	0.51	0.46	0.49	0.61	0.66	0.67	0.7	0.61	0.87	0.68	0.6	0.87	0.88
Gd	1.8	1.58	1.95	2.4	2.49	2.64	2.25	1.93	3.11	2.29	2.5	3.15	2.5
Tb	0.3	0.29	0.39	0.42	0.41	0.44	0.37	0.35	0.6	0.43	0.4	0.52	0.43

Tm	0.17	0.21	0.24	0.22	0.23	0.24	0.19	0.25	0.31	0.2	0.2	0.27	0.21
Yb	1.03	1.01	1.15	1.42	1.3	1.49	1.23	1.22	1.5	1.36	1.3	1.56	1.36
Lu	0.17	0.17	0.19	0.23	0.21	0.22	0.21	0.2	0.25	0.23	0.2	0.25	0.21
Hf	2.15	3.42	2.55	3.41	3.06	3.25	2.94	2.79	3.56	3.38	3	4.31	3.89
Ta	0.23	0.31	0.25	0.44	0.42	0.45	0.42	0.47	0.63	0.41	0.4	0.62	0.52
W	n.d.	1.4	<2.5	<2	<3.5	<2.7	1.3	<2.5	<2.7	<4.9	<3.2	<2.7	<3.5
Ir (ppb)	<1.9	<1.8	<2	<2.1	<2	<1.9	<1.4	<1.8	<2.5	<2.1	<1.8	<2.1	<2
Au (ppb)	1.1	<1.4	<1.1	0.4	<1.7	<1.7	<1.6	<1.4	<1.7	<2	<1.5	<1.7	0.4
Th	3.48	3.16	3.29	5.33	5.7	5.92	4.47	4.87	5.33	5.22	6.5	8.27	5.75
U	1.61	3.03	1.24	1.45	1.46	1.77	1.12	1.19	1.14	1.02	1.1	1.64	1.48

Notes: Abundances were determined by INAA and are given in parts per million (ppm) for most samples, or in weight percent (wt %) or parts per billion (ppb), where indicated. The standard deviation of each element at each sample site is noted after the sample's range of measurements.

Table 4. Soluble ion abundances of sediments from Cores 2074, 33, and 39 in Don Juan Basin, Antarctica, were determined by selective electrode or ion chromatography.

Core ID	2074	2074	2074	33	33	33	39	39	39
Depth (cm)	Na^+ (ppm)	Ca^{2+} (ppm)	Cl^- (ppm)	Na^+ (ppm)	Ca^{2+} (ppm)	Cl^- (ppm)	Na^+ (ppm)	Ca^{2+} (ppm)	Cl^- (ppm)
-0.5	860	490	1120	52.5	138	225	98.2	31.9	169.5
-1.5	112	395	700	45	108	207	264.9	38.8	350.5
-2.5	50	400	700	49.5	280	310	296.6	46	400.9
-3.5	76	410	720	56	340	450	146.4	57.9	209.5
-4.5	39	410	690	42	230	360	1987.5	60.7	2118.6
-5.5	36	410	690	40	280	380	3791.6	147.7	3826.6
-6.5	38	420	690	38	250	390	1848.9	185	1961.4
-7.5	32	360	610	33	230	305	406.7	133.5	532.3
-8.5	31	390	540	34	180	315	96.6	99.5	200.3
-9.5	28	350	490	32	210	305	68.2	66.3	105.7
-10.5	23	350	505	31	190	310	15.9	25.4	54.5
-11.5	23	320	490	31	225	340	18.3	15.1	47.5
-12.5	31	310	490	31	230	250	7.1	8.1	25.6
-13.5	30	300	490	30	135	240	33.5	9.2	38.5
-14.5	33	340	485	29	140	250	18.6	7.3	35.7
-15.5	33	310	500	12.5	130	250	18	6.9	33.3
-16.5	31	340	500	9.4	130	260	22.2	5.3	23.8
-17.5	32	360	500	7.2	115	215	18	6.2	23.3
-18.5	33	350	510	7.5	115	210	29.6	4.5	30.7
-19.5	29	250	445	6.6	120	220	55.6	6.3	22.6
-20.5	32	325	495	3.1	105	190	28.3	2.8	15.7
-21.5	33	355	480	10.8	160	310	11.1	2.7	9.3
-22.5	39	355	500	11	160	300	3.6	3.7	6.5
-23.5	29	290	395	9.4	150	265	8	3.6	13
-24.5	29	320	395	7.9	110	245			
-25.5	26	215	380	10.5	140	260			
-26.5	31	270	395	4	121	215			
-27.5	31	290	420						
-28.5	32	300	450						
-29.5	32	300	475						
-30.5	32	300	515						
-31.5	32	320	520						

Notes: Core 33 and 2074 data tables were unavailable; consequently data were carefully derived from an original hand drawing made by Everett Gibson. Core 39 data tables were available.

Table 5. Sample mineralogy (qualitative) as inferred from spectroscopy and as determined by XRD (qualitative) for Core 2074 (JB1124-1125), 33 (JB1129-1133), and 39 (JB1134-1138). Many samples contain poorly crystalline or short-range ordered hydrated phases that are difficult to identify and are listed in the perceived order of abundance.

Core #	Core ID	Sample Depth (cm)	Mineralogy from reflectance spectroscopy	Mineralogy from XRD
Core 2074, center of Don Juan Pond, appx. 116 m above sea level	**JB1126**	0-1	anhydrite, gypsum, calcite, ferrihydrite, quartz	anhydrite, gypsum, albite, quartz, augite, orthoclase
	JB1124	1-2	gypsum, anhydrite, ferrihydrite, quartz, calcite	gypsum, anhydrite, quartz, augite, ,
	JB1125	8-10	anhydrite, quartz, pyroxene, halite, thenardite, mica	quartz, albite, augite, orthoclase, epidote, gypsum, thenardite, halite
Core 33, 150 m SW of Core 2074, appx. 116.4 m above sea level	**JB1129**	0-1	quartz, pyroxene, mica	quartz, albite, orthoclase, thenardite, augite, anhydrite, halite, gypsum
	JB1130	3-4	quartz, pyroxene, mica, anhydrite	quartz, albite, orthoclase, thenardite, anhydrite, augite
	JB1131	8-10	quartz, pyroxene, mica, maybe anhydrite	quartz, albite, orthoclase, augite, anhydrite, gypsum
	JB1132	12-14	quartz, pyroxene, mica, anhydrite	quartz, albite, orthoclase
Core 39, 300 m SW of Core 2074, appx. 117 m above sea level	**JB1134**	0-1	quartz, feldspar, pyroxene, trace anhydrite	quartz, albite, augite, epidote, anhydrite

	JB1135	2-5	quartz, feldspar, pyroxene, gypsum, trace anhydrite	quartz, albite, thenardite, halite, epidote
	JB1136	6-8	quartz, feldspar, pyroxene, gypsum, aluminosilicates similar to allophane, calcite, trace anhydrite	quartz, albite, thenardite, orthoclase, magnetite, gypsum
Core 39, 300 m SW of Core 2074, appx. 117 m above sea level	**JB1137**	10-12	quartz, feldspar, pyroxene, aluminosilicates similar to allophane, calcite, trace anhydrite	quartz, albite, orthoclase, augite, magnetite, thenardite, gypsum
	JB1138	15-16	quartz, feldspar, pyroxene, chamosite, calcite, trace anhydrite	quartz, albite, augite, epidote, magnetite

Supplementary Materials

Table S1. Comparison of Na, K, and Fe oxides from INAA and XRF data. INAA oxide abundances were calculated from INAA elemental abundances. Unnormalized and INAA-normalized differences are calculated to assess method comparability. The standard deviation of each oxide at each sample site (for each analytical method) is noted after the sample's range of measurements.

	Depth (cm)	**1-2**	**8-10**	**0-1**	**3-4**	**8-10**	**12-14**	**16-20**	**0-1**	**2-5**	**6-8**	**10-12**	**15-16**
	Core ID	**JB1124**	**JB1125**	**JB1129**	**JB1130**	**JB1131**	**JB1132**	**JB1133**	**JB1134**	**JB1135**	**JB1136**	**JB1137**	**JB1138**
INAA	**Na_2O %**	1.04	1.05	2.83	2.14	2.2	1.87	1.88	2.55	5.49	2.99	2.68	2.76
XRF	**Na_2O %**	0.95	1.05	5.03	4.64	6.3	5.23	4.56	5.03	4.65	4.39	4.1	4.2
	Difference	0.09	0	-2.2	-2.5	-4.1	-3.36	-2.68	-2.48	0.84	-1.4	-1.42	-1.44
	Normalized differences	0.09	0	-0.77	-1.17	-1.87	-1.79	-1.43	-0.98	0.15	-0.47	-0.53	-0.52
INAA	**K_2O %**	0.74	0.7	1.54	1.33	1.43	1.36	0.96	1.53	1.2	1.91	1.08	1.73
XRF	**K_2O %**	0.71	0.9	2.49	2.03	2.02	1.77	1.88	2.31	5.25	3.14	2.47	2.54
	Difference	0.03	-0.2	-0.95	-0.7	-0.59	-0.41	-0.92	-0.78	-4.05	-1.23	-1.39	-0.81
	Normalized differences	0.04	-0.28	-0.61	-0.52	-0.41	-0.3	-0.95	-0.51	-3.36	-0.65	-1.28	-0.47
INAA	**Fe_2O_3 %**	3.44	4.02	4.16	4.23	3.69	4.13	3.69	5.44	4.58	3.87	4.54	4.37
XRF	**Fe_2O_3 %**	3.43	3.93	3.97	4.27	3.67	4.17	3.96	5.24	4.61	4.17	4.33	4.41
	Difference	0.01	0.09	0.19	-0.04	0.02	-0.04	-0.27	0.2	-0.03	-0.3	0.21	-0.04
	Normalized differences	0	0.02	0.04	-0.01	0.01	-0.01	-0.07	0.04	-0.01	-0.08	0.05	-0.01